ARTICLES

On the Dissociation of Aromatic Radical Anions in Solution. 1. Formulation and Application to *p*-Cyanochlorobenzene Radical Anion

Damien Laage,[†] Irene Burghardt,[‡] Thomas Sommerfeld,[§] and and James T. Hynes*[,†,#]

Département de Chimie, CNRS UMR 8640 PASTEUR, Ecole Normale Supérieure, 24 rue Lhomond, 75231 Paris Cedex 05, France, Département de Chimie, CNRS UMR 8642, Ecole Normale Supérieure, 24 rue Lhomond, 75231 Paris Cedex 05, France, Theoretische Chemie, Physikalisch-Chemisches Institut, Universität Heidelberg, Im Neuenheimer Feld 229, D-69120 Heidelberg, Germany, and Department of Chemistry and Biochemistry, University of Colorado, Boulder, Colorado 80309-0215

Received: June 10, 2003; In Final Form: September 26, 2003

A theoretical formulation is presented for the dissociation of aromatic radical anions in solution, $[Ar-X]^{\bullet-} \rightarrow Ar^{\bullet} + X^-$, and applied to the dissociation of the *p*-cyanochlorobenzene radical anion $[CN-\Phi-Cl]^{\bullet-}$ in several solvents. Key ingredients of the description are (i) the inclusion of the conical intersection (CI) aspects of the problem and (ii) the incorporation of nonequilibrium solvation (within a dielectric continuum solvent description). The CI feature is critical for this cleavage in the ground electronic state, because the required electronic coupling that allows the dissociation vanishes for a planar molecular geometry but is finite for finite C−Cl bending angle. The nonequilibrium solvation aspect is required, because of the inability of the solvent to equilibrate instantly to the changing molecular charge distribution during the radical anion dissociation process. These features are illustrated via the $[CN-\Phi-Cl]^{\bullet-}$ dissociation reaction path in a dimethylformamide (DMF) solvent, where C−Cl out-of-plane bending is required to avoid the CI intersection point, which leads to a bent transition state, and where the solvent is shown to reorganize prior to the crossing of the transition state. Reaction rate constants calculated via transition state theory (TST) are in reasonable agreement with experimental values in several solvents. It is also found that intrinsic activation free energies vary linearly with the homolytic bond dissociation energy of the radical anion, which is an experimentally observed feature. Comparison with previous descriptions is given, and inclusion of the CI features of the dissociation is shown to lead to large differences in the reaction activation free energy, which is related to the large electronic coupling, and the energetic cost to bend the C−Cl angle to reach the bent transition state. Possible improvements of the treatment, as well as extensions to other reaction problems, are discussed. Several of the theoretical constructs required for the reaction rate constants and reaction paths implemented in the present paper are developed in the second paper of this series, *On the Dissociation of Aromatic Radical Anions in Solution. 2. Reaction Path and Rate Constant Analysis*.

1. Introduction

The cleavage of an aromatic radical anion into the corresponding aromatic radical *Ar* plus an anionic nucleophile *X*,

$$[Ar-X]^{\bullet-} \rightarrow Ar^{\bullet} + X^- \qquad (1.1)$$

is important in a range of chemical contexts, most prominently for the $S_{R,N}1$ radical chain mechanism of nucleophilic substitution,[1−4] which is of major interest for organic synthesis and more generally connected with fundamental mechanistic questions in nucleophile−electrophile chemistry. Furthermore, aromatic radical anions are involved in the formation mechanism of Grignard reagents[5] and in DNA strand damage.[6] These dissociations have been the object of extensive investigation both in experiment—via electrochemical,[3,4,7−12] pulse radiolysis,[13−17] electron transmission spectroscopy[18−21] and electron spin resonance (ESR)[22] techniques—and in theory,[2,23−32] via assorted techniques. In this paper, we construct a theoretical description for this reaction class in solution and illustrate it via calculation of the reaction paths and rate constants for the thermal dissociation of the *p*-cyanochlorobenzene radical anion ($[CN-\Phi-Cl]^{\bullet-}$) in several solvents for which experimental rate data are available for comparison.

In this first effort, our efforts are focused on the phenyl ring class of aromatic radical anions (as opposed to, for example, a benzylic anion class). As shown in more detail within, this class is characterized by the presence of a *conical intersection* (CI), which has a crucial role in the dynamics. A CI is produced by the crossing of electronic curves in one geometry but is an avoided crossing at other geometries. Although such CIs are the subject of much current attention in a photochemical context[33−41]—where they provide a "funnel" that connects the excited electronic states with the ground state—there have been very few theoretical studies of the influence of a CI on a ground-

* Author to whom correspondence should be addressed. E-mail: hynes@chimie.ens.fr.
[†] Département de Chimie, CNRS UMR 8640 PASTEUR.
[‡] Département de Chimie, CNRS UMR 8642.
[§] Theoretische Chemie, Physikalisch-Chemisches Institut, Universität Heidelberg.
[#] University of Colorado.

10.1021/jp035637u CCC: $25.00
Published on Web 11/25/2003

state thermal reaction,[33,42,43] and none in the presence of the solvent. Therefore, the present work, together with our earlier communication,[44] provides the first theoretical study that examines the impact of a CI on a ground electronic state thermal reaction in solution. We draw attention to a very recent study by Lorance et al[43] on neutral *N*-methoxyheterocyclic radical dissociations, where CIs are also involved; these reactions were studied experimentally in solution and theoretically via vacuum electronic structure calculations (also see ref 17).

Our general approach is one that has already been followed by one of us for a variety of solution-phase charge-transfer reactions that involves bond breaking and/or bond making,[45] or more generally involving strong participation of reacting solute nuclear coordinates.[46] Vacuum electronic structure calculations are used to generate certain electronically nonadiabatic valence bond (VB) energy curves and the electronic coupling between them. The latter are then applied in a formulation that includes nonequilibrium solvation by the surrounding polar solvent. This nonadiabatic perspective allows a formulation which incorporates the critical feature[47] that the solution phase adiabatic wave functions differ electronically from their vacuum values, because of electrostatic interactions of the reacting solute with the polar solvent molecules. As will be shown, the electronic coupling for the radical anion dissociation is large, which is a typical and crucial feature for bond-breaking reactions, in strong contrast to the simpler weak coupling situation for outer-sphere electron-transfer reactions.[48,49] The nonequilibrium solvation description is required by the feature that, typically, the solvent is out of equilibrium during the rapid passage through the reaction transition-state (TS) region.[45] This important feature has not been adressed in those few semiempirical electronic structure treatments of aromatic radical anion dissociations that include solvation,[25,30,50,51] which, instead, adopt an equilibrium solvation perspective.

Compared to other ground-electronic-state unimolecular dissociations studied via this basic approach,[45b−f] the phenylic radical anion case is distinguished by the CI phenomenon, which is an aspect that also distinguishes the present work from the pioneering theoretical studies by Savéant,[2,4,8,23] as discussed within. With respect to the electronic structure aspects of the problem, several semiempirical calculations exist,[25,26] as do several vacuum ab initio studies.[27,30−32,43,52] However, the latter addresses neither the critical CI nor the solvation aspects, whereas the former methodology, as will be shown, unfortunately is generally unable to accurately and usefully describe even the vacuum system in planar geometry, necessitating the present ab initio approach. (In special circumstances, however, semiempirical calculations can still be useful, vide infra.) A distinctive and important feature of these ab initio calculations is that they address the critical issue of the vacuum autoionization of the radical anions; the anions are unstable, with respect to electron detachment ($[ArX]\bullet^- \rightarrow ArX + e^-$) in the vacuum,[19] which is an aspect that requires special techniques.

The outline of the remainder of this paper is as follows. Section 2 involves a variety of general considerations, including issues of the electronic states involved and the electronic coupling (and the key coordinate involved: the C−Cl bend) to produce the CI features, as well as the choice of the paradigm molecule ($[CN-\Phi-Cl]\bullet^-$) for study. In Section 3, we present the results of vacuum ab initio calculations, which provide the explicit essential required ingredients, such as the diabatic energy curves and the coupling between them, culminating in the picture of the ground adiabatic potential energy surface with a bent transition state for the reference vacuum dissociation. Section 4 addresses the radical anion dissociation in solution, where the reaction actually occurs, including the basic formulation and the evaluation of the ingredients required for its application. Calculation of the anion dissociation rate constants in several solvents is presented in Section 5, as are comparisons with experiment. The similarities and differences of our approach and previous work are also discussed. Concluding remarks are given in Section 6.

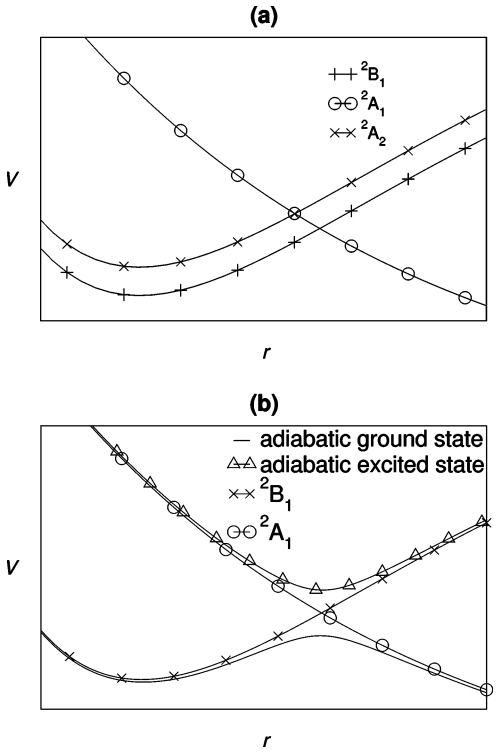

Figure 1. Schematic electronic-state patterns and energies for a phenyl radical anion versus the dissociation coordinate *r*: (a) in the planar geometry and (b) in a bent geometry. NB: in some compounds, the $^2B_1$ state may not be below the $^2A_2$ state (see Section 2.3).

In a companion paper[53] (hereafter referenced as "II"), we analyze the reaction paths and rate constant ingredients in detail.

2. General Considerations

In this section, we discuss some key aspects of the electronic states that are involved in the dissociation, together with assorted criteria resulting in the selection of a particular radical anion for the present study.

2.1. Electronic States. Three electronic states are to be considered for the thermal radical anion dissociation (eq 1.1). The first two are the π^* states that arise from the degenerate lowest unoccupied molecular orbital (LUMO) state of benzene, noting that the degeneracy is lifted upon adding a substituent in the ring. These states are labeled $^2A_2$ and $^2B_1$ in C_{2v} geometry, i.e., referring to a planar reference geometry of the molecule. For such π^* states, the excess electron is localized mainly in the ring. The remaining state is the one with σ^* excitation, namely $^2A_1$. Here, the excess electron is essentially localized in the C−*X* bond and the $^2A_1$ state leads to dissociation of an X^- ion, i.e., $(Ar-X)\bullet^- \rightarrow Ar\bullet + X^-$; asymptotically, this $^2A_1$ state thus corresponds to the phenyl radical ground state.[54] The three potential energy curves are schematically illustrated in Figure 1a, for a situation of planar geometry and with $^2B_1$ being more stable than $^2A_2$.

All these electronic states are autoionizing in the gas phase, i.e., the process $(Ar-X)\bullet^- \rightarrow (Ar-X) + e^-$ intervenes, resulting in lifetimes on the order of femtoseconds.[19,55,56] However, in

Figure 2. Simplified schematic for the $a_2\pi^*$ and $a_1\sigma^*$ orbitals (left), and the $b_1\pi^*$ and $a_1\sigma^*$ orbitals (right).

solution, autoionization should not have a role, because of the stabilization of the ion by the polar solvent, and the much slower dissociation process dominates.[57,58]

2.2. Electronic Coupling. For a phenyl radical anion in planar C_{2v} geometry, there is no $\pi^*-\sigma^*$ electronic coupling, and a symmetry-breaking coordinate motion is required for a finite coupling inducing an avoided crossing and allowing the reaction (cf. Figure 1b). These are just the conditions to have a CI between the potential energy surfaces that correspond to either the $^2A_2$ or $^2B_1$ state and the dissociative $^2A_1$ state.

The symmetry-forbidden nature of the cleavage in planar geometry was noted long ago for $[\Phi-Cl]\bullet^-$ in the gas phase.[28,59] In a manner that is similar to that for haloethylene radical anions, the $\pi^*-\sigma^*$ intramolecular electron transfer occurs via $\pi^*-\sigma^*$ vibrational coupling.[20,60] This symmetry-breaking motion was suggested to correspond to the out-of-plane halogen wag;[8,20] this was confirmed in the case of $[\Phi-Cl]\bullet^-$ by recent gas-phase experiments[32] and calculations,[31] which showed that this out-of-plane vibration strongly couples the $^2B_1$ and $^2A_1$ states.[61] Qualitatively, this can be understood by considering the $a_2\pi^*$, $b_1\pi^*$, and $a_1\sigma^*$ orbitals (Figure 2): there is no overlap between the pairs $a_2\pi^*/a_1\sigma^*$ and $b_1\pi^*/a_1\sigma^*$ in C_{2v} geometry, but an out-of-plane displacement of the halogen leads to a nonvanishing overlap, and thus mixing, between the $b_1\pi^*$ and $a_1\sigma^*$ orbitals.[62] Thus, the reaction model that we develop within this work centers on the out-of-plane wagging coupling mode, and its explicit inclusion is one of the novel aspects of our treatment.[44,63]

Thus, a relatively simple two-state picture emerges, involving $^2B_1-^2A_1$ coupling, provided that several conditions are fulfilled: (i) the $^2B_1$ state is the radical anion ground state; (ii) the $^2B_1$ and $^2A_2$ states are reasonably well-separated, such that the $^2A_2$ state is not thermally accessible; and (iii) the anion equilibrium geometry is planar, such that the states mix only in the course of the dynamical process. We next try to select a suitable "paradigm molecule" for our study, guided by the conditions described in points (i)−(iii), which prevent the situation from becoming exceedingly complex.

2.3. Choice of "Paradigm Molecule". Our paradigm molecule choice will be the *p*-cyanochlorobenzene radical anion $[CN-\Phi-Cl]\bullet^-$, as described below. Readers who are only immediately interested in the result of that choice may safely proceed to Section 2.4.

Condition (i) requires that the $^2B_1$ state should be much more stable than the $^2A_2$ state. In benzene, these two states are degenerate; therefore, this assurance will be achieved through the addition of one or more substituent(s) on the ring, with well-chosen inductive- and resonance-donating or withdrawing properties. Because the inductive effect involves the σ electrons close to the substituent, it affects the $^2B_1$ and $^2A_2$ states in a similar fashion but not the dissociative $^2A_1$ state. On the other hand, the resonance effect affects the π system that neighbors the substituent: in the $^2A_2$ state, the orbital exhibits a node on the substituent-bearing C atom, whereas, in the $^2B_1$ state, the electronic density is high on this C atom; therefore, the resonance effect only influences the $^2B_1$ state. Those qualitative predictions have been experimentally confirmed for radical anions for several substituents.[19,55]

With these considerations in mind, we first consider the simplest anion, which has only a halogen substituent, e.g., the chlorobenzene radical anion. The Cl atom already lifts the $^2B_1-^2A_2$ degeneracy; however, it is only a weak resonance donor and the $^2B_1$ and $^2A_2$ states are still almost degenerate. This is confirmed experimentally[21] and by our ab initio calculations, which are presented elsewhere,[63] which show, in addition, that there is a fundamental difficulty with $[\Phi-Cl]\bullet^-$ for our present purposes.[64] In contrast to the neutral species,[65] these ab initio results indicate that there is *no* equilibrium geometry for the anion: the ground state is nonbonding, first bending and then dissociating without any barrier.[66,67]

Because conditions (ii) and (iii) are thus not satisfied for the simple chlorobenzene anion, we look for the adequate substituent for the paradigm compound.[68,69] The nitro substituent is ruled out, because its strength as an inductive withdrawer is so strong and stabilizes the $^2B_1$ state so much more than the $^2A_1$ state that the dissociation can occur on the same time scale as other bimolecular processes.[2,8,14] The acetophenone radical anion could be another candidate, because its cleavage is well-documented experimentally;[8,15,16,70] however, this system is too large to be studied with the required ab initio methods. The *p*-cyanochlorobenzene radical anion $[CN-\Phi-Cl]\bullet^-$ is another potential paradigm molecule. Indeed, the resonance withdrawer effect of the cyano should ensure that the reactant ground state is $^2B_1$, whereas its inductive withdrawer power should lead to a dissociation reaction that is neither diffusion-limited nor in competition with other processes. These qualitative considerations are confirmed both experimentally, where the measured rate constant is in the 10^7-10^9 s^{-1} range,[8,9,12,13,71−73] and by our ab initio calculation results described in Section 3.2.1, which indicate that $^2B_1$ is 9 kcal more stable than $^2A_2$. Furthermore, the calculated equilibrium geometry is planar,[74] in contrast to $[\Phi-Cl]\bullet^-$.

From the aforementioned considerations, we select $[CN-\Phi-Cl]\bullet^-$, for the following reasons. For this species, we know from the ab initio calculations (to be discussed in Section 3.2) that (i) the $^2B_1$ state is the electronic ground state, (ii) this state is sufficiently separated from the $^2A_2$ state, and (iii) the ground-state geometry is planar. These are the basic requirements for an analysis in terms of a two-state model, with the electronic coupling of $^2B_1-^2A_1$ allowing the dissociation that was developing during the dynamics (see the end of Section 2.2). Furthermore, the dissociation rate should be sufficiently high that other deactivation routes for the anion do not have any roles, and experimental rate data are available in several room-temperature solvents for comparison.[8,9,12,13,70−73,75]

2.4. Diabatic versus Adiabatic Representation. The generally split adiabatic surfaces (see Figure 1b) are defined in the conventional sense, i.e., as solutions to the electronic Schrödinger equation, in the Born−Oppenheimer approximation, thus corresponding to the results obtained from electronic structure calculations. Focusing solely on the ground (g) and (first) excited

(e) adiabatic states, the wave functions are $\Psi_g(r,\theta)$ and $\Psi_e(r,\theta)$, where r denotes the distance between the chlorine and the proximate ring carbon, and θ is the angle between the ring plane and the C−Cl bond. In this representation, the nonadiabatic coupling between $\Psi_g(r,\theta)$ and $\Psi_e(r,\theta)$ is then of kinetic-energy type; it becomes singular at a CI, which makes this representation computationally inconvenient.[41d]

A more convenient representation for the present purposes is the *diabatic* representation. Focusing only on the coupled states in Figure 1, the diabatic wave functions would be $\psi^B(r,\theta)$ and $\psi^A(r,\theta)$. The adiabatic-diabatic representation connection is then

$$\Psi_{g,e} = c^B_{g,e}(r,\theta)\,\psi^B(r,\theta) + c^A_{g,e}(r,\theta)\,\psi^A(r,\theta) \qquad (2.1)$$

where the c parameters are appropriate geometry-dependent coefficients. The explicit construction of a suitable diabatic representation in the vicinity of a CI has been much discussed.[39,41b−e] In the diabatic picture, the surfaces vary with respect to a "tuning" coordinate (here, the carbon−halogen separation r, which is located at the crossing of the two surfaces (cf. Figure 1), and they are coupled and split by a potential-like term that depends on the coordinate associated with the "coupling mode", in our case, the wag angle θ. This electronic coupling, here called β, arises from the mixing of π^* and σ^* orbitals, as discussed in Section 2.2 in bent geometries.

We construct a diabatic model for the coupled energy surfaces pertaining to the radical anion dissociation in a vacuum,[76] of the following form:

$$V(r,\theta) = \begin{pmatrix} V^B(r,\theta) & \beta(\theta) \\ \beta(\theta) & V^A(r,\theta) \end{pmatrix} \qquad (2.2)$$

such that the ground and excited adiabatic potentials are

$$V_{g,e}(r,\theta) = \frac{V^B(r,\theta) + V^A(r,\theta)}{2} - \frac{1}{2}\sqrt{(V^A(r,\theta) - V^B(r,\theta))^2 + 4\beta(\theta)^2} \qquad (2.3)$$

Here, the B and A superscripts refer to the uncoupled (i.e., in the absence of any electronic coupling) $^2B_1$ and $^2A_1$ states. Thus, we have the vacuum diabatic potentials $V^B(r,\theta)$ and $V^A(r,\theta)$ and the vacuum coupling $\beta(\theta)$.

A convenient prescription to define the diabatic states explicitly relies on a Taylor expansion of the adiabatic surfaces about the CI. It is often sufficient to include a coupling term linear in the coupling mode, i.e.,

$$\beta(\theta) = b\theta \qquad (2.4)$$

with the coupling parameter b obtained from the slope of the adiabatic surfaces as the degeneracy is lifted away from $\theta = 0$.[41c] The fact that linear coupling gives the dominant effect is characteristic of many CI problems.[41d−f,77]

In general, β should also be regarded as a function of the C−Cl bond length r, presumably increasing as r decreases, for fixed finite angle θ, because of the increasing $\pi^*-\sigma^*$ overlap. Unfortunately, we have no information from the ab initio calculations about this dependence, and we have no method that we consider reliable to estimate it. Its impact near the planar reactant geometry should not be important, because the coupling will vanish due to its θ dependence. At large separations r, where the coupling should vanish as the orbital overlap vanishes, our treatment will overestimate the coupling; however, because the $^2B_1-^2A_1$ gap also increases at large r values, the impact should not be serious (and large r values are, in any event, not our focus). However, the impact in the transition-state (TS) neighborhood may not be completely negligible, and this limitation must be kept in mind.

In our formulation, we will use the aforementioned simple diabatic representation, with the understanding that the corresponding parameters will be eventually obtained from electronic structure calculations for the vacuum *adiabatic* surfaces (see Section 3). In particular, when using the "tuning mode" r and "coupling mode" θ as the vacuum coordinates, the information required in the linearized scheme consists of (i) the adiabatic potential slopes at $\theta = 0$ (C_{2v} geometry), i.e., $\kappa_{g,e} = (\partial V_{g,e}/\partial r)_{r=r_{CI}}$, and (ii) the parameter b in eq 2.4, giving the linear increase $2b$ of the gap between the adiabatic surfaces at the CI: $\Delta V = V_e(r_{CI},\theta) - V_g(r_{CI},\theta) \approx 2b\theta$. With these parameters, the adiabatic/diabatic mixing angle, which is defined[41c] as $\chi(r,\theta) = {}^1/_2 \arctan\{2b\theta/[(\kappa_g - \kappa_e)r]\}$ determines the adiabatic/diabatic transformation,

$$\Psi_g = \cos\chi(r,\theta)\psi^B(r,\theta) - \sin\chi(r,\theta)\psi^A(r,\theta)$$
$$\Psi_e = \sin\chi(r,\theta)\psi^B(r,\theta) + \cos\chi(r,\theta)\psi^A(r,\theta) \qquad (2.5)$$

which is a more explicit version of eq 2.1.

2.5. Analytic Diabatic Potential Models. For the discussion of the gas-phase surfaces, and especially for the treatment of the solution-phase reaction, we require analytic representations for the diabatic potentials V^B and V^A in eq 2.3.

For the energy variation in phenyl-halogen coordinate r, we adopt a Morse potential for the $^2B_1$ state, and an exponential dissociative potential for the $^2A_1$ state. To both of these potentials, we add a harmonic potential for the wag coordinate, with the same force constant for the $^2B_1$ and $^2A_1$ states. Hence,

$$V^B(r,\theta) = V_0^B + D_e^B\{1 - \exp[-a^B(r - r_{eq}^B)]\}^2 + \frac{1}{2}k_\theta\theta^2$$
$$V^A(r,\theta) = V_0^A + D_e^A \exp(-a^A r) + \frac{1}{2}k_\theta\theta^2 \qquad (2.6)$$

Several approximations are involved in eq 2.6, which we now discuss.

We have assumed that the potential along θ is purely harmonic for the diabatic states. A quartic component may be added, which would become dominant for large θ angles.[78] However, for the TS geometries, we will find, in Section 3.3, that the angle remains relatively small (<30°); therefore, incorporation of such a component does not seem to be critical.

We have also assumed that the force constant k_θ is the same in the bound $^2B_1$ state and in the dissociative $^2A_1$ state. However, the charge distribution found in Section 3.2 is different in those two states: for the $^2B_1$ state, the charge is delocalized on the entire aromatic ring, whereas for the $^2A_1$ state, the charge is more localized on the Cl group. Because the $^2A_1$ state is dissociative, the force constant is probably somewhat smaller than that in the $^2B_1$ bound state.

Finally, we have assumed that the wag force constant k_θ in eq 2.6 is independent of the dissociation coordinate r. In fact, it must decrease at large r, where there is no longer any restoring torque for the angular motion of the Cl atom.[79] However, the fractional extension of r from its equilibrium value to its TS value in solution is on the order of 10%, and this neglect should not be grossly in error.

3. Gas-Phase Surfaces

In this section, we examine the gas-phase aspects of the radical anion dissociation problem; we describe the electronic

structure methodology that has been used, the vacuum potential energy curves and the coupling between them, and the force constant for the C−Cl bend. The two-dimensional ground-state surface is then discussed, together with the rate constant.

3.1. Ab Initio Methodology. Semiempirical methods were proven to be unreliable when applied to the different systems considered in Section 2.3. In particular, as already noted for a related compound in the work by Fontanesi,[80] the semiempirical $^2A_1$ state is erroneously predicted to be bound along r,[25b,63] but it corresponds to a dissociative σ^* state. In addition, in the $[\Phi-Cl]^{\bullet-}$ case, semiempirical methods yield a stable reactant geometry,[25b] in contradiction with the result of the more-refined ab initio methods detailed below.

This forces the utilization of ab initio methodology for the $[CN-\Phi-Cl]^{\bullet-}$ anion. However, a difficulty does exist, from the ab initio perspective: all the electronic states are autoionizing in the gas phase ($[\Phi-X]^{\bullet-} \rightarrow \Phi-X + e^-$, i.e., with lifetimes on the femtosecond scale.[19,55] In contrast, autoionization should not have a role in solution, because of solvent stabilization of the anion. Therefore, it would be convenient to refer to a "modified vacuum Hamiltonian", with the autoionization process inhibited, as done in Section 2.4. The difficulty is then to perform ab initio calculations in such a way that the system is stabilized (i.e., the electronic states become bound) but the potential energy surfaces are not modified in an uncontrolled way.

Among the different suitable techniques that are available to study autoionizing species, we adopted the "complex absorbing potentials" (CAPs) method.[81] The idea is to allow autoionization but to absorb the escaping electron by the CAP, which is an absorbing potential $-iW$ that is added to the physical Hamiltonian H:

$$H(\eta) = H - i\eta W \tag{3.1}$$

where W is typically a real "soft" boxlike potential in the electron dissociation coordinate R and η is a strength parameter. The eigenvalues of $H(\eta)$ correspond to the complex Siegert energies of the resonant states:

$$E_{res} = E_r - i\left(\frac{\hbar}{2\tau}\right) \tag{3.2}$$

where E_r is the real part of the energy that we will use in the solution model, and τ is the state lifetime.

The first step of the computation is a self-consistent field (SCF) calculation on the neutral molecule, performed with the MOLCAS5 package[82] with Dunning's double-ζ basis set[83] augmented with one d-type polarization function and a (1s6p)/[1s5p] set of diffuse functions on the heavy atoms. The resonance-state wave functions are then constructed from the set of all configurations that describe the N-electron target plus an extra electron: $(\text{target})^N(n\phi^*)^1$, where ϕ^* is an orbital of appropriate symmetry. Thus, the target electrons are frozen in their SCF orbitals, and, loosely speaking, this static-exchange assumption is analogous to Koopmans' theorem[84] for positive electron affinities.

The specific CAP form that we used is the box-CAP that was suggested by Santra et al.,[85] where the CAP box size has been set to the maximum component of the respective nuclear coordinates plus 2.5 bohr in each Cartesian direction. The CAP Hamiltonian is then diagonalized repeatedly for different CAP strengths η. All described resonance states can be identified at all investigated geometries from the η-trajectories of their complex energies that stay close to the real axis and show stabilization cusps.

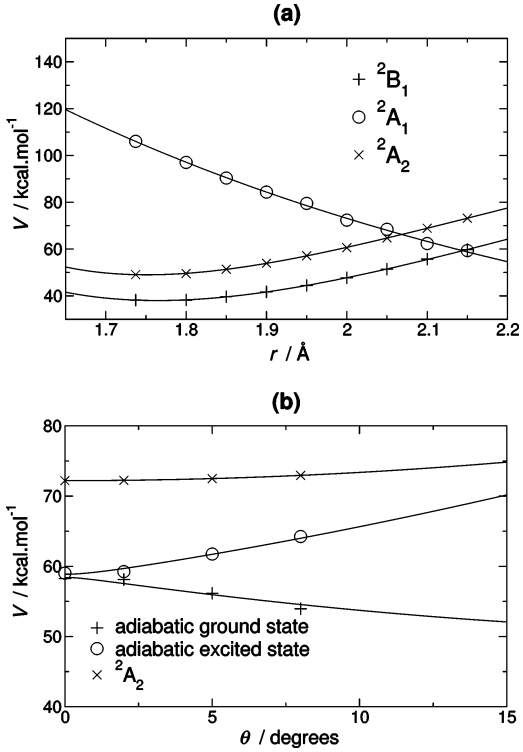

Figure 3. Fitted ab initio data for $[CN-\Phi-Cl]^{\bullet-}$ (a) along r for $\theta = 0$ and (b) along θ for r values similar to its value at the conical intersection (CI).

TABLE 1: Parameters of the Morse and Dissociative Exponential Forms Used for the $^2B_1$, $^2A_2$, and $^2A_1$ States[a] of $[CN-\Phi-Cl]^{\bullet-}$

	value		
parameter	$^2B_1$ state	$^2A_1$ state	$^2A_2$ state
V_0 (kcal)	38	−7	49
D_e (kcal)	114	1074	108
a (Å^{-1})	1.47	1.29	1.60
r_{eq}^B(Å)	1.76		1.75

[a] See eq 2.6.

3.2. Ab Initio Results. *3.2.1. Results.* Ab initio data points have been calculated for the three electronic states $^2B_1$, $^2A_2$, and $^2A_1$, along r for $\theta = 0$, i.e., in the planar geometry, and along θ for r similar to its value at the CI (see Figure 3). These data have been fitted using eqs 2.6 and 2.4, with the fit parameters collected in Table 1.

The $^2B_1$ state is the anion electronic ground state and lies well below the $^2A_2$ state, which is a feature anticipated in the discussion of Section 2.3 (concerning substituent effects). The ab initio calculated $^2B_1-^2A_2$ gap is ∼9 kcal and remains almost constant over a range of r distances between the equilibrium geometry and the $^2B_1/^2A_1$ intersection point (see Figure 3c).

To a good approximation, the gap between the coupled $^2A_1$ and $^2B_1$ states increases linearly along the angle θ, as assumed for the diabatic coupling $\beta(\theta) = b\theta$ (cf. eq 2.4); the gap is given by $\Delta(\theta) = 2b\theta$, and one can determine the coupling parameter b value, given in Table 2.

3.2.2. Force Constant for the Out-of-Plane Bend. The potentials along θ also serve to determine the force constant k_θ in the assumed harmonic out-of-plane bend potential $V_\theta = {}^1/_2 k_\theta \theta^2$. We now discuss several pieces of information that allow us to fix a range of values that we would expect for k_θ.

In terms of ab initio calculations, we only have force constant information on the $^2A_2$ state. Indeed, in the $^2B_1$ and $^2A_1$ states, for small θ values, the potential energy contribution from the

TABLE 2: Characteristic Data for [CN−Φ−Cl]•⁻

parameter	value
gap between $^2B_1$ and $^1A_1$ states at $r_0(B_1)$, Δ^a	63 kcal
wag force constant in the bound uncoupled $^2A_2$ state, $k_\theta(^2A_2)$	23 cal/deg^2
coupling parameter, b	0.62−0.75 kcal/deg
equilibrium position parameter, x^b	0.53
vacuum reaction energy, $\Delta_r V$	−45 kcal

[a] $\Delta = |V^A(r^B_{eq}, 0) - V^B(r^B_{eq}, 0)|$. See ref 116. [b] $x = 2b^2/(k_\theta\Delta)$.

TABLE 3: Charges and Dipole Moments in the Different Electronic States of [CN−Φ−Cl]•⁻, Each Fixed in Its Equilibrium Geometry for the Neutral[a]

state	charge q_{Cl}	charge q_{ring}	charge q_{CN}	dipole moment, μ (D)
neutral	0.02	0.13	−0.15	2.9
$^2B_1$	−0.12	−0.55	−0.33	5.1
$^2A_2$	−0.08	−0.69	−0.23	3.6
$^2A_1$	−0.43	−0.34	−0.23	3.2

[a] The origin of the dipole moments is the center of mass.

quadratic bend potential $^1/_2 k_\theta\theta^2$ is so small, compared to the linear electronic coupling energy $b\theta$, that no reliable information on k_θ can be extracted from the fit of the ab initio data. The θ curvature of the A_2 state, evaluated at $r = r_{CI}$, is reported in Table 2. We consider this to be a lower bound, because the force constant should decrease somewhat as r increases.[86]

Another estimate for k_θ can be obtained by a normal-mode analysis at the anion equilibrium geometry and the approximation that the wagging local-mode frequency can be identified with the relevant normal-mode frequency. This leads to an estimate of $k_\theta \simeq 34$ cal/deg^2, to be compared to the value $k_\theta \simeq 23$ cal/deg^2 that was just estimated using the $^2A_2$ state curvature.[63]

In conclusion, it would seem reasonable to consider a force constant range of 23−34 cal/deg^2, with a preference for the former value of 23 cal/deg^2.

The reduced mass for the θ coordinate is the moment of inertia of the Cl atom in its angular motion, which depends on the ring−Cl-group distance, r. For simplicity, we fix its value at that for the transition state (TS).[87]

3.2.3. Charge Distributions. Finally, our calculations provide some information on the charges and dipole moments that are associated with the different electronic states of [CN−Φ−Cl]•⁻, which will be exploited for the solution calculation, because they govern the important reacting solute−solvent interaction. The calculations provide estimates for the atomic charges and the dipole moments for the different electronic states, all data being for the $^2B_1$ state equilibrium geometry (cf. Table 3).

We will consider the neutral cyanochlorobenzene molecule for comparison, where we find that the Cl atom is practically neutral, whereas in all electronic states of the anion, it is more negative than in the neutral, and substantially moreso in the dissociative $^2A_1$ state (although Table 3 indicates that, in the latter, the Cl charge is not −1; we will return to this point in Section 4). At the same time, the dipole moment is much larger in this state. The data for the $^2B_1$ and $^2A_2$ states are not identical but are similar to each other. As will be discussed in Section 4.2, the solvation energies for these two bound states are mainly due to the total point charge, whose magnitude is similar in the two states, and the dipole moment difference will be too small to change the bound-state ordering. Therefore, $^2B_1$ should remain lower in energy than $^2A_2$ in solution; this important conclusion will allow us to continue to focus in solution on the $^2B_1$ and $^2A_1$ states. The detailed impact of the [CN−Φ−Cl]•⁻ charge distribution on the reaction characteristics will be described in detail in Section 4.

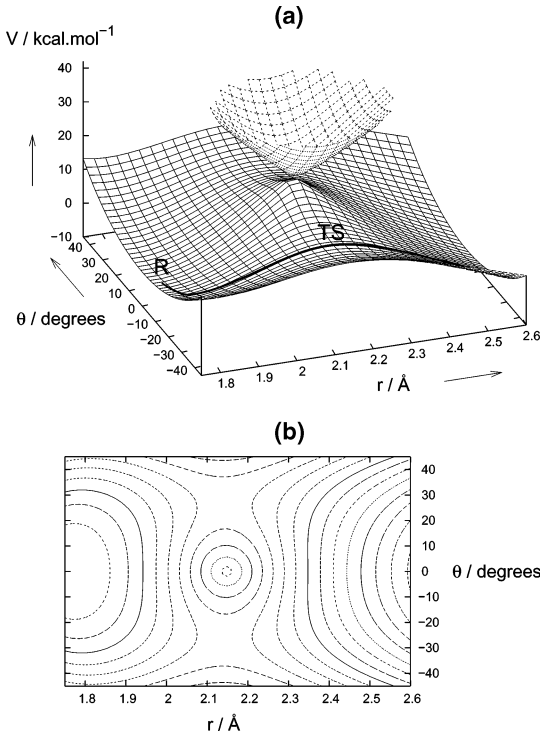

Figure 4. Gas-phase potential energy surface for [CN−Φ−Cl]•⁻ with $k_\theta = 28$ cal/deg^2: (a) three-dimensional representation and (b) contour plot with a 2 kcal spacing between two successive contour lines. (Note that the actual well in θ for large r values should be softer in θ, because we assumed the k_θ force constant to be independent of r.) The trajectory plotted in panel a corresponds to the virtual gas-phase dissociation, which never occurs, because the electron ejection is faster.

TABLE 4: Influence of the Force Constant (k_θ) and the Coupling Parameter (b) on the Gas-Phase Transition State Location, Prefactor A_{vac}, Activation Energy ($\Delta V^\ddagger$), and Rate Constant (k_{300K})

k_θ (cal/deg^2)	b (kcal/deg)	$r^\ddagger$ (Å)	$\theta^\ddagger$ (deg)	A_{vac} ($\times 10^{13}$ s^{-1})	$\Delta V^\ddagger$ (kcal/mol)	k_{300K} (s^{-1})
23	0.62	2.14	27	1.7	12.8	7.5×10^3
35	0.62	2.14	19	1.9	15.6	7.2×10^1
23	0.75	2.14	33	1.1	8.9	3.5×10^6

3.3. Ground Adiabatic Potential in the Gas Phase. The gas-phase potential energy surface for [CN−Φ−Cl]•⁻, using the results and considerations of Sections 3.2.1 and 3.2.2, is shown in Figure 4. Although, as noted in Sections 2.1 and 3.1, the anion will autoionize in the gas phase, this surface is, nonetheless, instructive.

The topology corresponds to a CI: there is an actual surface crossing in planar geometry and avoided crossings in all "cuts" of the potential surfaces for $\theta \neq 0$. During the course of the thermal dissociation, the CI is approached "from below", and the cone topology deflects the trajectories. In the parlance of Robb et al.,[33] it corresponds to a "peaked conical intersection with a horizontal moat", where the dynamics is confined to the "moat" of the CI, which is a perspective previously discussed by Rettig in connection with twisted intramolecular charge-transfer reactions in solution.[88]

Because the trajectories are forced to circumscribe the cone, the process is *adiabatic*: the electronic coupling influence is predominant over that of the wag force constant.[89] At the CI, when θ increases from zero, the energy decrease due to the stabilization by the increasing coupling is larger than the energy increase, because of the moving away from the wag harmonic

potential's equilibrium position. However, for very large angle values, because, by assumption, the coupling is linear, and the wagging potential is quadratic in θ, the potential increases again (see Figure 4).

Table 4 collects the rate constants that are calculated in the transition state theory (TST) description[90] and are derived in II:

$$k = 2\left(\frac{\omega_{\|}^{R}}{2\pi}\right)\left(\frac{\omega_{\perp}^{R}}{\omega_{\perp}^{\ddagger}}\right)\exp\left(-\frac{\Delta V^{\ddagger}}{k^{B}T}\right)$$
$$= A_{vac}\exp\left(-\frac{\Delta V^{\ddagger}}{k^{B}T}\right) \quad (3.3)$$

which involves the perpendicular normal-mode frequency $\omega_{\perp}^{\ddagger}$ at the bent transition state and the mode frequencies $\omega_{\|}^{R}$ and $\omega_{\perp}^{R}$ parallel and perpendicular to the reaction path in the reactant. There are two independent and symmetric transition states, located at $+\theta^{\ddagger}$ and $-\theta^{\ddagger}$, because the Cl atom can wag either above or below the ring plane. These two paths are independent, because they are very far apart—e.g., in the most reasonable case in Table 4, $\theta^{\ddagger} \simeq \pm 27°$—which is the origin of the factor of 2 in eq 3.3.

The aforementioned vacuum results will be used in Section 5 to gain perspective on the reaction in solution—where the reaction actually occurs—and we limit our remarks here to two important points. First, we note that, at the transition state, the parallel (i.e., along the reaction path) and perpendicular normal modes almost coincide with the r and θ modes, respectively. As we will see, this need not be the case in solution. Second, the electronic coupling magnitude only depends on the angle θ in our description. In our range of k_θ and b values, the coupling at the vacuum TS varies between $\beta = 12$ kcal/mol and 25 kcal/mol, such that the reaction always remains very strongly electronically adiabatic. This order of magnitude of electronic coupling is consistent with other reactions that involve bond breaking.[45a−c]

4. Solution-Phase Reaction

4.1. Formulation. *4.1.1. General Perspective.* We now turn to the formulation of the radical anion dissociation problem in solution, where the reaction actually occurs, for which we adopt a dielectric continuum solvent model. There are two key ingredients beyond the gas-phase issues addressed and information obtained in the previous sections: the electronic structure of the reacting solute, and the nonequilibrium state of the solvent.

The first ingredient centers on the fundamental feature that the anion's electronic structure, at different values of the separation r and the bending angle θ, is altered in the presence of a polar solvent, compared to the vacuum. Thus, for example, one cannot simply consider that the anion at different points of the calculated electronically adiabatic surface shown in Figure 4 should simply now be solvated. A natural way to describe the actual state of affairs is to retain the diabatic perspective of Section 2.4. In the vacuum, the adiabatic wave function is generated by the mixing of the diabatic wave functions by the electronic coupling, as in eqs 2.1 and 2.5. In solution, the mixing of these states to produce the adiabatic state is, in addition, influenced by electrostatic interactions with the solvent, because of the *different* charge distributions associated with these diabatic states. Thus, the ground (adiabatic) electronic wave function of the anion in solution is a different linear combination of the vacuum diabatic wave functions than that in the vacuum.

The second ingredient concerns the nonequilibrium polarization state of the solvent. Although much theoretical work involves the characterization of the electronic structure of a solute in equilibrium with the surrounding solvent[91]—the solvent polarization is in equilibrium with the solute's charge distribution at all times—this is generally inappropriate. In the present problem, the critical solute nuclear motions involved in the reaction dynamics are too rapid for the solvent to remain in equilibrium with the dissociating anion's changing charge distribution, and nonequilibrium solvation must be addressed.

The solvent nonequilibrium polarization state is characterized in our description by the solvent coordinate s, described further below, which gauges the electric nuclear (e.g., orientational) polarization in the solvent. Because one coordinate is a reduced description compared to a full many-body description, the solution surfaces of interest are free-energy, rather than energy, surfaces, whose composition is now described.

We continue to adopt the diabatic perspective for the radical anion, and the solution electronically ground and excited-state adiabatic wave functions are expressed as linear combinations of the vacuum diabatic wave functions

$$\Psi = c^{B}(r,\theta,s)\,\psi^{B}(r,\theta) + c^{A}(r,\theta,s)\,\psi^{A}(r,\theta) \quad (4.1)$$

where the coefficients $c^{B}(r,\theta,s)$ and $c^{A}(r,\theta,s)$ depend on the solvent coordinate s. Thus, the composition of the adiabatic states in solution, in terms of ψ^{B} and ψ^{A}, depends on the solvent coordinate s, which gauges the solvent polarization. In such a description, solvent effects are added in terms of a diagonal contribution $G^{B,A}$ that is dependent on s,[92,93]

$$G(r,\theta;s) = \begin{pmatrix} V^{B}(r,\theta) + \Delta G_{s}^{B}(r,\theta,s) & \beta(\theta) \\ \beta(\theta) & V^{A}(r,\theta) + \Delta G_{s}^{A}(r,\theta,s) \end{pmatrix}$$
$$= \begin{pmatrix} G^{B}(r,\theta,s) & \beta(\theta) \\ \beta(\theta) & G^{A}(r,\theta,s) \end{pmatrix} \quad (4.2)$$

such that the ground-state free-energy surface is

$$G_{g}(r,\theta,s) = \frac{G^{B}(r,\theta,s) + G^{A}(r,\theta,s)}{2} - \frac{1}{2}\sqrt{(G^{A}(r,\theta,s) - G^{B}(r,\theta,s))^{2} + 4(\beta(\theta))^{2}} \quad (4.3)$$

in analogy to the gas-phase version in eq 2.3. Because we will only be concerned with the ground state, we drop the subscript g notation. The occupation probabilities of the diabatic states $[c^{B,A}(r,\theta,s)]^2$ in the adiabatic solution wave function shown in eq 4.1 are given by

$$[c^{B,A}(r,\theta,s)]^{2} = \frac{1}{2}\left[1 \pm \frac{G^{A}(r,\theta,s) - G^{B}(r,\theta,s)}{\sqrt{(G^{A}(r,\theta,s) - G^{B}(r,\theta,s))^{2} + 4(\beta(\theta))^{2}}}\right] \quad (4.4)$$

Here, $V^{B,A}(r,\theta)$ are the diabatic state vacuum energies (see Section 2.4), whereas $\Delta G_{s}^{B,A}(r,\theta;s)$ are additional free-energy contributions that result from the interaction of the diabatic-state charge distribution with the solvent polarization, and the "self free energy" of the solvent (which is related to the interaction between the electric polarization in two small elements of the solvent, summed over the elements). If the solvent polarization were in equilibrium with the charge distribution of the diabatic state (B, A), then $\Delta G_{s}^{B,A}(r,\theta;s)$ would reduce to the equilibrium solvation free energy $\Delta G_{s,eq}^{B,A}$.[94]

We will decompose $\Delta G_s^{B,A}$—and, thus, $G^{B,A}$—into equilibrium and nonequilibrium solvation contributions below.

We pause to note that our basic perspective, and the results which follow from it below, has been previously applied to VB wave functions,[45,46,96] which are particular diabatic wave functions, each with a definite *fixed* charge distribution (or at least one that, even if varying with an internal coordinate such as r, is independent of the solvation[97]); the latter requirement would guarantee that the wave functions ψ^B and ψ^A in eq 4.1 are precisely independent of s. Here, we apply the formulation to the diabatic states we have previously discussed; the issue of any possible solvent dependence of the charge distribution of the reacting system, and thus of ψ^B and ψ^A, will be discussed in Section 4.2.1.

4.1.2. Diabatic Free Energies. We now outline the development to find the form of the diabatic free energies $G^{B,A}(r,\theta,s)$, extending the basic procedure of Lee and Hynes[98] and Borgis and Hynes[92] to the anion dissociation. A dielectric continuum model is used for the solvent. It is assumed that the electronic polarization of the solvent is equilibrated around any relevant charge distribution of the solute, because of the rapid time scale of the solvent molecule electrons. On the other hand, the orientational polarization—because of the dipole moments of the polar solvent molecules—is not generally so equilibrated; thus, we must consider general nonequilibrium orientational polarization fields $\boldsymbol{P}_{or}(\boldsymbol{x})$, where $\boldsymbol{x}$ indicates a field point in the solvent.

In the special case that the orientational polarization is equilibrated to the solute's charge distribution, the latter with internal coordinates r and θ, in either diabatic state $^2B_1$ or $^2A_1$, then an equilibrium orientational polarization $\boldsymbol{P}_{or,eq}^{B,A}(\boldsymbol{x}; r,\theta)$ exists in the solvent, and the free energy is the equilibrium one: $G_{eq}^{B,A}(r,\theta)$. Here, the (r,θ) dependence arises because, for example, in the $^2A_1$ state, the location of the negatively charged Cl^- anion will be different for different r and θ values. In the general case, the free energies are functionals of the polarization field $\boldsymbol{P}_{or}(\boldsymbol{x})$:

$$G^{B,A}(r,\theta,[\boldsymbol{P}_{or}(\boldsymbol{x})]) = G_{eq}^{B,A}(r,\theta) + \frac{1}{2}k_s^\circ \int d\boldsymbol{x}\, [\boldsymbol{P}_{or}(\boldsymbol{x}) - \boldsymbol{P}_{or\,eq}^{B,A}(\boldsymbol{x}; r,\theta)]^2 \quad (4.5)$$

in which

$$k_s^\circ = 4\pi\left(\frac{1}{\epsilon_\infty}\right)\left(\frac{1}{(1/\epsilon_\infty)} - (1/\epsilon)\right) \quad (4.6)$$

which involves the static dielectric constant ϵ and high-frequency dielectric constant ϵ_∞, is a force constant that gauges the difficulty of having an orientational polarization fluctuation away from the appropriate equilibrium value. The dielectric constant combination $((1/\epsilon_\infty) - (1/\epsilon))$ is a characteristic for that polarization (see, for example, refs 48 and 98).

We now assume that, for the anion dissociation, the relevant nonequilibrium $\boldsymbol{P}_{or}(\boldsymbol{x})$ throughout the reaction process is a linear combination of the equilibrium polarization fields for $^2B_1$ and $^2A_1$:

$$\boldsymbol{P}_{or}(\boldsymbol{x}) = (1 - z)\,\boldsymbol{P}_{or,eq}^{B}(\boldsymbol{x}; r,\theta) + z\boldsymbol{P}_{or,eq}^{A}(\boldsymbol{x}; r,\theta) \quad (4.7)$$

The variable z thus specifies the orientational polarization state of the solvent and can be regarded as a solvent coordinate. Thus, for small z, the polarization is more similar to that appropriate to the $^2B_1$ state, whereas for z values that approach unity, it is more similar to that appropriate to the $^2A_1$ state. Using eq 4.7, the nonequilibrium diabatic free energies given in eq 4.5 are

$$G^B(r,\theta,z) = G_{eq}^B(r,\theta) + \frac{1}{2}k_s(r,\theta)z^2$$
$$G^A(r,\theta,z) = G_{eq}^A(r,\theta) + \frac{1}{2}k_s(r,\theta)(z-1)^2 \quad (4.8)$$

where we have introduced a new solvent force "constant", $k_s(r,\theta)$,

$$k_s(r,\theta) = k_s^\circ \int d\boldsymbol{x}\, [\boldsymbol{P}_{or,eq}{}^A(\boldsymbol{x}; r,\theta) - \boldsymbol{P}_{or,eq}{}^B(\boldsymbol{x}; r,\theta)]^2 \quad (4.9)$$

which, however, is dependent on the solute internal variables r and θ, because the equilibrium polarizations are dependent on them.

Using eq 4.8 in conjunction with eq 4.3 for the adiabatic free energy G, it is easy to show that the derivative of G, with respect to the solvent coordinate z (using eq 4.4), is given by

$$\frac{\partial G(r,\theta,z)}{\partial z} = k_s(r,\theta)[z - c^A(r,\theta,z)^2] \quad (4.10)$$

so that when the solvent is in equilibrium at any given r and θ, and this derivative vanishes, the solvent coordinate is equal to the square equilibrium A component of the adiabatic wave function:

$$z_{eq} = [c_{eq}^A(r,\theta,z_{eq})]^2 \quad (4.11)$$

More generally, one should regard the electronic composition at a fixed r and θ as a function of z, via eqs 4.4 and 4.8.

For qualitative purposes, the aforementioned description, in terms of z, would be sufficient. However, for the anion dissociation, we will calculate the rate constant, and, in II, the reaction path; both calculations require the inclusion of the kinetic energy $K_{or} \propto \int d\boldsymbol{x}\, [\dot{\boldsymbol{P}}_{or}(\boldsymbol{x})]^2$, which is associated with the polarization field $\boldsymbol{P}_{or}(\boldsymbol{x})$, where the dot indicates time differentiation. Using eq 4.7, because of the r- and θ-dependent equilibrium polarizations, this leads to cross terms in kinetic energy, e.g., a cross term that involves $\dot{z}\dot{r}$. Thus, the terms z, r, and θ are not dynamically independent variables, which very greatly complicates the analysis. However, as shown in II, a *new* solvent coordinate s can be defined in which the kinetic energy is diagonal in $\dot{s}$, $\dot{r}$, $\dot{\theta}$, circumventing this difficulty. As detailed in that work, we assume that the charge distributions of the $^2B_1$ and $^2A_1$ states are not sensitive to θ, and that the $^2B_1$-state charge distribution (centered in the aromatic ring) does not change with the C−Cl extension r, such that the $^2B_1$-state equilibrium polarization is independent of r and θ, and the $^2A_1$ state equilibrium polarization is independent of θ:

$$\frac{\partial \boldsymbol{P}_{or,eq}^B}{\partial r} = \frac{\partial \boldsymbol{P}_{or,eq}^B}{\partial \theta} = 0$$
$$\frac{\partial \boldsymbol{P}_{or,eq}^A}{\partial \theta} = 0 \quad (4.12)$$

i.e., the equilibrium functional dependences are

$$\boldsymbol{P}_{or,eq}^B(r,\theta) = \boldsymbol{P}_{or,eq}^B(r_{eq}^B)$$
$$\boldsymbol{P}_{or,eq}^A(r,\theta) = \boldsymbol{P}_{or,eq}^A(r) \quad (4.13)$$

with r_{eq}^B being the equilibrium C−Cl bond extension in the B state of the anion.

The solvent coordinate s then is given by

$$s = z\sqrt{\frac{k_s(r)}{k_s(r_{eq}^B)}} \tag{4.14}$$

in which k_s (given in eq 4.9), by the aforementioned assumptions, is now only a function of r, and $k_s(r_{eq}^B)$ is its value evaluated at the equilibrium geometry of the radical anion in the B state. It will prove more convenient to re- express these parameters in terms of reorganization energies, whose significance is explained below:

$$\lambda_s(r) = \frac{1}{2}k_s(r)$$

$$\lambda_s = \frac{1}{2}k_s(r_{eq}^B) \tag{4.15}$$

where the latter is just the former evaluated at the B-state solute equilibrium geometry. The expression for $\lambda_s(r)$ from eqs 4.15 and 4.9, with the relations given in eqs 4.13, is

$$\lambda_s(r) = \frac{2\pi}{\epsilon_\infty[(1/\epsilon_\infty) - (1/\epsilon)]}\int d\boldsymbol{x}\,[\boldsymbol{P}_{or\,eq}^A(\boldsymbol{x}; r) - \boldsymbol{P}_{or,eq}^B(\boldsymbol{x}; r_{eq}^B)]^2 \tag{4.16}$$

Using eqs 4.14 and 4.15 (together with eq 4.9), the free energies presented in eq 4.5 can now be expressed in terms of the solvent coordinate s, via our working equations:

$$G^{B,A}(r,\theta,s) = V^{B,A}(r,\theta) + \Delta G_{s,eq}^{B,A}(r) + \lambda_s(s - s_{eq}^{B,A}(r))^2 \tag{4.17}$$

$$\Delta G_{s,eq}^B(r) = \Delta G_{s,eq}^B(r_{eq}^B) \tag{4.18}$$

where we have now expressed the equilibrium free energies in terms of their two components, $V^{B,A}(r,\theta)$, which is the diabatic-state vacuum energy (cf eq 4.2), and $\Delta G_{s,eq}^{B,A}(r,\theta)$, which is the equilibrium solvation free energy for the solute geometry (r,θ). Consistent with eq 4.13, the equilibrium solvation free energies for the anion in the diabatic states are independent of θ, with that for the $^2B_1$ state having no r dependence, whereas the r dependence is retained for $\Delta G_{s,eq}^A(r)$, which corresponds to the different degree of equilibrium solvation as the Cl moiety moves away from the ring in the $^2A_1$ state; as discussed later in Section 4.2.1, this involves a redistribution of the charge between the ring and the Cl atom.

The net consequence for these free energies of the shift to the new solvent variable s description is that there are harmonic contributions for the nonequilibrium polarization terms, centered at the equilibrium positions $s_{eq}^{B,A}(r)$ of s for the anion reaction system in the $^2B_1$ and $^2A_1$ states:

$$s_{eq}^B(r) = 0$$

$$s_{eq}^A(r) = \sqrt{\frac{\lambda_s(r)}{\lambda_s(r_{eq}^B)}} \tag{4.19}$$

These expressions follow from the definitions in eqs 4.14 and 4.15, together with eq 4.9 and the evaluations of eq 4.7 at the appropriate equilibrium polarizations for the $^2B_1$- and $^2A_1$-state solutes, with the assumptions given in eq 4.12. An additional important feature of the s coordinate description is that the force constant, $2\lambda_s = k_s(r_{eq}^B)$, for the nonequilibrium polarization terms is a constant that is *independent* of the anion system internal variables r and θ.

The equilibrium positions $s_{eq}^{B,A}(r)$ defined in eqs 4.19 have the following significance. When the anionic system is in the $^2B_1$ diabatic state, the equilibrium solvent coordinate value $s_{eq}^B = 0$ denotes an equilibrium solvent polarization condition appropriate to the equilibrium geometry $r = r_{eq}^B$. When the solute is in the $^2A_1$ diabatic state, the equilibrium polarization changes as charge is redistributed between the ring and the Cl atom as the latter moves away; this is ultimately reflected in eq 4.19 via the r-dependent $\lambda_s(r)$ factor. We must stress that this shift, which will be more fully discussed in Section 4.2, is within the diabatic $^2A_1$ state. The charge shift for the reaction itself is a consequence of the electronic coupling between the diabatic $^2B_1$ and $^2A_1$ states; i.e., it occurs in the electronically adiabatic ground state.

Similarly, we emphasize that these equilibrium positions are for the diabatic states. For the adiabatic case, there is only one equilibrium solvent coordinate position s_{eq} for a given r and θ, which, from eqs 4.14 and 4.11, is

$$s_{eq}(r,\theta) = [c_{eq}^A(r,\theta,s_{eq})]^2\sqrt{\frac{k_s(r)}{k_s(r_{eq}^B)}} \tag{4.20}$$

Generally, the electronic composition is given by eq 4.4, together with eqs 4.17 and 4.18.

4.1.3. Diabatic Free Energy Discussion. Equations 4.15−4.19 complete the reformulation of the diabatic free energies $G^{B,A}(r,\theta,s)$, in terms of the new solvent variable s.

The schematic behavior of the diabatic free energies presented in eq 4.17 is illustrated in Figure 5. We consider the two-dimensional (r, s) perspective, in which the geometry is planar ($\theta = 0$). At any other fixed angle, the bending potential $^1/_2k_\theta\theta^2$ would be added and would thus simply add a constant term to all displayed curves. In the ensuing discussion, we describe these curves, focusing on the issues of the solvent equilibrium positions and force constants.

In panel a of Figure 5, we focus on the dissociation coordinate r behavior, with the solvent coordinate transverse. The vacuum contributions $V^{B,A}(r,\theta = 0)$ for the bound and dissociative states are indicated by the dashed curves. In a polar solvent, the constant equilibrium solvation free energy $\Delta G_{s,eq}^B(r_{eq}^B)$ for the $^2B_1$ state, with the charge localized in the ring system, lowers the vacuum curve $V^B(r,\theta = 0)$ uniformly. The solvent coordinate equilibrium position is $s_{eq}^B = 0$, and the nonequilibrium solvation contribution well, $\lambda_s(s - s_{eq}^B)^2 = \lambda_s s^2$, is indicated as a transverse well. In regard to the dissociative diabatic $^2A_1$ state in panel a, along the line $s = s_{eq}^A(r)$, where the solvent is equilibrated to the dissociating anion $^2A_1$ state at each r, the equilibrium solvation free energy $\Delta G_{s,eq}^A(r)$ lowers the vacuum curve $V^A(r,\theta = 0)$ by an increasing amount as the $C-Cl^-$ coordinate increases. For ease of representation, we only label this stabilization at a convenient geometry r_{CIP}^A that corresponds to a contact ion pair (CIP). At any r, the nonequilibrium solvation contribution $\lambda_s[s - s_{eq}^A(r)]^2$ is a transverse well with a (constant) force constant $k_s = 2\lambda_s$, with its minimum located at $s = s_{eq}^A(r) = \sqrt{\lambda_s(r)/\lambda_s}$, as indicated in Figure 5a only at the CIP geometry.

In panel b of Figure 5, we display the solution situation in the solvent coordinate s, at the two different values of r, labeled in panel a. The two diabatic solvent curves are displayed at the $^2B_1$-state equilibrium geometry $r = r_{eq}^B$; these two curves were represented as transverse in panel a. The two solvent wells have

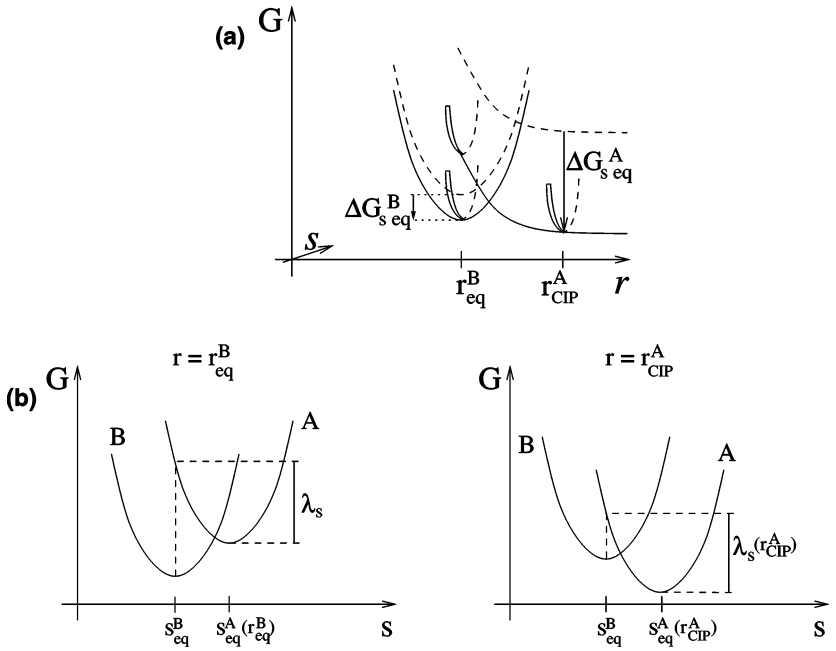

Figure 5. Schematic picture of the definitions of $\Delta G_s^{B,A}$ and λ_s, showing free-energy curves of the $^2B_1$ and $^2A_1$ states along (a) the dissociation coordinate r and (b) the solvent coordinate s in the reactant and product geometries. In both cases, the geometry is kept planar. Legend for the upper panel is as follows: (− − −) in the vacuum and (—) in a polar solvent.

different equilibrium positions but the same force constant $2\lambda_s$. Indeed, this figure identifies λ_s as the so-called solvent reorganization energy at $r = r_{eq}^{B}$. As indicated in the left-hand panel of Figure 5b, the latter is defined in terms of a Franck−Condon transition from the bottom of the $^2B_1$ curve to the $^2A_1$ curve, at the $^2B_1$-state equilibrium solvent coordinate value $s = s_{eq}^{B} = 0$, followed by the solvent reorganization to the minimum of the $^2A_1$-state curve:

$$\begin{aligned}\lambda_s &= G^A(r_{eq}^B, s = s_{eq}^B = 0) - G^A(r_{eq}^B, s = s_{eq}^A[r_{eq}^B]) \\ &= G^A(r_{eq}^B, s = s_{eq}^A[r_{eq}^B]) + \frac{2\lambda_s}{2}[s_{eq}^A(r_{eq}^B)]^2 - \\ &\qquad G^A(r_{eq}^B, s = s_{eq}^A[r_{eq}^B]) \\ &= \frac{2\lambda_s}{2}[s_{eq}^A(r_{eq}^B)]^2 \\ &= \lambda_s\left[\frac{\lambda_s(r = r_{eq}^B)}{\lambda_s(r = r_{eq}^B)}\right] = \lambda_s \end{aligned} \tag{4.21}$$

On the other hand, at a different r value, e.g., $r = r_{CIP}^{A}$ in the right-hand side of panel b in Figure 5, the reorganization energy is different, because the equilibrium solvent position for the $^2A_1$ state differs from $r = r_{eq}^{B}$:

$$\begin{aligned}\lambda_s(r = r_{CIP}^A) &= G^A(r_{CIP}^A, s = s_{eq}^B = 0) - \\ &\qquad G_{eq}^A(r_{CIP}^A, s = s_{eq}^A[r_{CIP}^A]) \\ &= \frac{2\lambda_s}{2}\left(\frac{\lambda_s(r = r_{CIP}^A)}{\lambda_s}\right) \end{aligned} \tag{4.22}$$

Equations 4.21 and 4.22 both are special cases of the general relationship

$$\begin{aligned}\lambda_s(r) &= G^A(r, s = s_{eq}^B = 0) - G_{eq}^A(r, s = s_{eq}^A[r]) \\ &= \frac{2\lambda_s}{2}[s_{eq}^A(r) - s_{eq}^B(r)]^2 \end{aligned} \tag{4.23}$$

with $s_{eq}^B(r) = s_{eq}^B(r_{eq}^B) = 0$.

This completes the discussion of the diabatic free energies G^A and G^B. The desired ground-state adiabatic free-energy surface $G(r,\theta,s)$ is given in terms of these energies in eq 4.3.

4.2. Solution-Model Specification. In this subsection, we examine the specifics of the modeling of the solvation aspects of the rate problem, first discussing the equilibrium solvation and then the nonequilibrium solvation features that are required in the overall free energy $G(r,\theta,s)$ expression (cf. eq 4.3 and eqs 4.15−4.19). Several features are common to both. The solvation is treated by considering the molecule to be composed of two cavities that are embedded in the dielectric continuum solvent: one centered on the aromatic ring, the other on the Cl moiety. In the bound $^2B_1$ state, the negative charge is mainly in the ring cavity, and in the dissociative $^2A_1$ state, it is mainly in the Cl cavity (to a degree that depends on r; see below). Dissociation then involves a charge transfer from the ring cavity to the Cl cavity, which is allowed by the $^2B_1-^2A_1$ electronic coupling, and the dominant effect of solvation is due to the charge-solvent interaction. In the treatment below, any dependence of any solvation on the wag angle is neglected, which is consistent with our model specifications in Section 4.1.2.

4.2.1. Equilibrium Solvation Free-Energy Formulation. We first consider the equilibrium solvation free energies, which, from eqs 4.17 and 4.18, are

$$\Delta G_{s,eq}^B(r_{eq}^B) = -\frac{2\pi}{\epsilon_\infty^{\,2}}\left[\frac{1}{(1/\epsilon_\infty) - (1/\epsilon)}\right]\int d\boldsymbol{x}\,[\boldsymbol{P}_{or}^{\,B}(\boldsymbol{x}; r_{eq}^B)]^2 - 2\pi\left[\frac{1}{1 - (1/\epsilon_\infty)}\right]\int d\boldsymbol{x}\,[\boldsymbol{P}_{el}^{\,B}(\boldsymbol{x}; r_{eq}^B)]^2$$

$$\Delta G^{A}_{s,eq}(r) = -\frac{2\pi}{\epsilon_\infty{}^2}\left[\frac{1}{(1/\epsilon_\infty) - (1/\epsilon)}\right]\int d\boldsymbol{x}\,[\boldsymbol{P}_{or}{}^{A}(\boldsymbol{x}; r)]^2 - 2\pi\left[\frac{1}{1-(1/\epsilon_\infty)}\right]\int d\boldsymbol{x}\,[\boldsymbol{P}_{el}{}^{A}(\boldsymbol{x}; r)]^2 \quad (4.24)$$

in terms of the orientional and electronic polarization fields $\boldsymbol{P}^{B,A}_{or,el}(\boldsymbol{x})$. These are as follows:

$$\boldsymbol{P}^{B}_{or,eq}(\boldsymbol{x}) = \frac{\epsilon_\infty}{4\pi}\left(\frac{1}{\epsilon_\infty} - \frac{1}{\epsilon}\right)\boldsymbol{E}^{B}(\boldsymbol{x}; r^{B}_{eq})$$

$$\boldsymbol{P}^{B}_{el,eq}(\boldsymbol{x}) = \frac{1}{4\pi}\left(1 - \frac{1}{\epsilon_\infty}\right)\boldsymbol{E}^{B}(\boldsymbol{x}; r^{B}_{eq})$$

$$\boldsymbol{P}^{A}_{or,eq}(\boldsymbol{x}; r) = \frac{\epsilon_\infty}{4\pi}\left(\frac{1}{\epsilon_\infty} - \frac{1}{\epsilon}\right)\boldsymbol{E}^{A}(\boldsymbol{x}; r)$$

$$\boldsymbol{P}^{A}_{el,eq}(\boldsymbol{x}; r) = \frac{1}{4\pi}\left(1 - \frac{1}{\epsilon_\infty}\right)\boldsymbol{E}^{A}(\boldsymbol{x}; r) \quad (4.25)$$

where $\boldsymbol{E}^{B,A}$ are the vacuum electric fields that result from the charge distributions of the reacting solute in the $^2B_1$ and $^2A_1$ states. Substituting eq 4.25 into eq 4.24, the equilibrium free energies of solvation can be directly expressed in terms of the vacuum electric fields:

$$\Delta G^{B}_{s,eq}(r^{B}_{eq}) = -\frac{1}{8\pi}\left(1 - \frac{1}{\epsilon}\right)\int d\boldsymbol{x}\,[\boldsymbol{E}^{B}(\boldsymbol{x}; r^{B}_{eq})\cdot\boldsymbol{E}^{B}(\boldsymbol{x}; r^{B}_{eq})]$$

$$\Delta G^{A}_{s,eq}(r) = -\frac{1}{8\pi}\left(1 - \frac{1}{\epsilon}\right)\int d\boldsymbol{x}\,[\boldsymbol{E}^{A}(\boldsymbol{x}; r)\cdot\boldsymbol{E}^{A}(\boldsymbol{x}; r)] \quad (4.26)$$

where the electronic and orientational contributions have been combined. The $(1 - (1/\epsilon))$ factor here reflects the feature that both the electronic and orientation polarizations are equilibrated; the static dielectric constant ϵ gauges the total polarization in equilibrium.

We evaluate these in terms of the Born model of solvation,[48c] in which the equilibrium solvation free energy of a unit charge in a cavity can be expressed as

$$\Delta G_s(\epsilon) = -\frac{1}{8\pi}\left(1 - \frac{1}{\epsilon}\right)\int d\boldsymbol{x}\,[\boldsymbol{E}(\boldsymbol{x})\cdot\boldsymbol{E}(\boldsymbol{x})] \quad (4.27)$$

where $\boldsymbol{E}(\boldsymbol{x})$ is the vacuum field due to the charge. Evaluation for a spherical cavity gives the well-known result[48c]

$$\Delta G_s(\epsilon) = -\frac{e^2}{2a}\left(1 - \frac{1}{\epsilon}\right) \quad (4.28)$$

in terms of the static dielectric constant ϵ of the solvent, the elementary charge e, and the cavity radius a, which is the key ingredient that must be assigned for each of the two cavities of the $[CN-\Phi-Cl]\bullet^-$ model. The specification of the cavities is discussed next.

4.2.2. Cavity Model Specification. This specification proves to be somewhat long and complex; readers who are more interested in the results that follow from the specification may proceed directly to Section 5.

4.2.2.1. Dissociative $^2A_1$ State. For very large r values, the adiabatic ground state asymptotically tends toward the $^2A_1$ diabatic dissociative state, and there is a full negative charge in the Cl cavity and no charge in the ring cavity. However, for smaller r values, the orbital that accommodates the excess electron is transforming from an atomic 3p orbital localized on the Cl atom to a molecular σ^* orbital, delocalized over the Cl atom and the ring C atom that it is approaching.

TABLE 5: Solvent Static and High-Frequency Dielectric Constants (ϵ and ϵ_∞, Respectively), Solvation Free Energies (ΔG_s), and Estimated Chlorine and Ring Cavity Sizes (a_{Cl} and a_Φ, Respectively) for $[CN-\Phi-Cl]\bullet^-$ in Water, Dimethyl Formamide (DMF), and Acetonitrile (MeCN)

	value		
parameter	water	MeCN	DMF
ϵ[a]	78.4	37.5	36.7
ϵ_∞[a]	1.78	1.80	2.04
ΔG_s (Cl^-) (kcal/mol)	−83[b]	−73[c]	−71[c]
ΔG_s ($CN-\Phi^-$) (kcal/mol)	−62[d]	−57[e]	−56[e]
a_{Cl} (Å)	1.97	2.21	2.25
a_Φ (Å)	2.65	2.85	2.90

[a] Dielectric constants from ref 117. [b] Hydration free energies from ref 117. [c] Solvation free energies in DMF and MeCN from the hydration free energies, and the transfer free energies from ref 117. [d] Solvation free energy from ref 105, plus the difference between the hydration free energies of Cl^- in refs 117 and 105. [e] No transfer free energies were available for $\Phi-CH_2^-$; it was estimated from the values from ref 117 for anions that have similar hydration free energies (I^- and SCN^-).

As confirmed by the ab initio calculations, for the $^2A_1$ electronic state in the $^2B_1$ equilibrium geometry, the Cl charge is only approximately −0.4 (see Table 3). Most of the remaining negative charge is on the C atom that bears the Cl atom, and receives approximately half of the electronic density of the σ^* orbital. This explains the significantly negative charge on the ring in the $^2A_1$ state reported in Table 3. The $^2A_1$ state charges thus depend on the bond length r, as modeled by an exponential decay, $q^{A}_{Cl}(r) = -1 + q_0\exp(-r/d)$. The parameter values, $q_0 = 3.2$ and $d = 0.9$ Å, are obtained from AM1[99] semiempirical calculations with configuration interaction between five states, performed with AMPAC[100] for different bond lengths r, and in a planar geometry, where the obtained adiabatic states coincide with the diabatic states.

In addition, these calculations show that the cyano endgroup charge remains approximately constant when the C−Cl bond is stretched. Even at very large r values ($\simeq 5$ Å, i.e., well past the transition state (TS)), the CN charge in the diabatic $^2A_1$ state has ultimately decreased in magnitude by only ∼25%; the approximate constancy of the $^2A_1$-state CN charge from the reactant to the TS region is evidently associated with the fact that, as discussed previously, the major rearrangements in the $^2A_1$ state are associated with rearrangements in the C−Cl moiety, far from the CN. Therefore, we assume that the CN group charge remains constant ($q_{CN} = -0.28$), and we approximate it to be identical in both the $^2A_1$ and $^2B_1$ states, which is an approximation that has been shown to be reasonable by the AM1 calculations. The cyano endgroup thus generates no difference in the equilibrium solvation free energies of the two states, and no solvent reorganization occurs around it during the charge transfer. Its only effect is to reduce the magnitude of the charge transfer between the ring and the Cl atom. The ring cavity charge is eventually deduced as $q^{A}_{\Phi}(r) = -1 - q^{A}_{Cl}(r) - q_{CN}$.

The Cl cavity radius is determined by the requirement that the Born solvation free energy fit the experimental hydration free energy of the Cl^- anion. For the ring cavity, we use an estimate based on the benzyl anion with a full negative charge in the cavity. For simplicity, we assume that the cavity sizes are independent of the magnitude of the charge in the cavity. The cavity sizes in water, dimethyl formamide (DMF) and acetonitrile (MeCN) are reported in Table 5. It is an unavoidable

TABLE 6: Calculated Charge Distributions for $^2B_1$ [CN−Φ−Cl]•⁻ Ground State in the Gas Phase and in Water, Acetonitrile (MeCN), and Dimethyl Formamide (DMF) Solvents (ab Initio Results from Table 3)

		charge distribution		
environment	method	q_{Cl}	q_{ring}	q_{CN}
vacuum	ab initio	−0.12	−0.55	−0.33
vacuum	AM1 − C. I. 5	−0.14	−0.57	−0.29
water	AM1 − C. I. 5 − SM2	−0.07	−0.57	−0.36
water	AM1 − C. I. 5 − COSMO	−0.07	−0.55	−0.38
MeCN	AM1 − C. I. 5 − COSMO	−0.08	−0.54	−0.38
DMF	AM1 − C. I. 5 − COSMO	−0.08	−0.54	−0.38

feature of this type of modeling that the cavity size changes with the solvent. In the three solvents considered, the radius of the ring cavity was estimated to be larger than that of the Cl^- anion cavity (cf Table 5). At this point, we stress the importance of the relative sizes of the Cl and ring cavities, because these will determine which diabatic state is preferentially stabilized in a polar solvent.

4.2.2.2. Bound $^2B_1$ State. In the planar geometry, the $^2A_1-^2B_1$ state coupling vanishes, and the adiabatic ground state coincides with the $^2B_1$ state. Thus, the charge distribution of our model diabatic $^2B_1$ state must match that of the adiabatic ground state in planar geometry. These charges have already been calculated ab initio in the vacuum (see Table 3), but they should be altered in solution. We estimate the polar solvent influence on the charge distribution via semiempirical calculations in a model dielectric continuum solvent, via standard procedures.[91] We have already noted in Section 3.1 that semiempirical calculations are generally not reliable for radical anions; therefore, we stress that the semiempirical charge distribution is only used as a guide. Nonetheless, when used in the vacuum and compared with the ab initio results, the semiempirical results seem to yield satisfactory charges (see Table 6).

Two different solvent models were used for the water solvent, and the different models led to similar charge distributions; the main trend is a shift of the electronic distribution from Cl^- toward CN^-. (Similar results are found for acetonitrile and DMF solvents; see Table 6.) However, this observation raises the issue first mentioned in Section 4.1.1, concerning the identification of the diabatic states as VB states,[97] with the latter having the characteristic features that the charge distribution, at any given molecular geometry, is fixed. If the $^2B_1$ diabatic state were truly a VB state, solvation would change its free energy, compared to that in the vacuum, but would not change the charge distribution. However, Table 6 has shown that the internal charge distribution of the $^2B_1$ state is changed by solvation. We must conclude that the diabatic $^2B_1$ state cannot be strictly represented as a single VB structure. Evidently, a detailed description would require at least two VB states, each with a fixed charge distribution, whose contribution in solution would be shifted compared to that in the vacuum. One could imagine, for example, two VB structures with all the negative charge not in the ring on the CN and one where that excess charge was on the Cl atom. Although one could consider a generalization to include this feature, the extra complexity required is very considerable.[45d,95] However, judging from Table 6, the vacuum−solution charge shift is not extensive; therefore, we will simply adopt a value of $q^B_{Cl} = -0.12$ in the following discussion as the diabatic $^2B_1$-state fixed distribution.

Therefore, the equilibrium solvation energy of the $^2B_1$ state will involve a partial charge in the Cl cavity and a partial charge in the ring cavity. The Cl and ring cavity sizes are assumed to be the same as those in the $^2A_1$ state (see Table 5).

With such cavity radii, in the ground-state equilibrium geometry, the two cavities will overlap, because, from our ab initio calculations, the distance between the ring center and the C atom is $d_{CC} = 1.41$ Å and the C−Cl equilibrium distance is 1.76 Å, so that the distance between the two cavity centers is 3.17 Å. This would bring us into a regime where the separate cavity approach is definitely no longer valid. To address this situation, we have decided to rescale the cavity radii while also rescaling the solvation energies, to keep the values of those energies unchanged; this could be considered to be a rescaling of the dielectric constant. We rescale the two cavity radii so that their sum is equal to the distance between the two cavity centers in the ground-state equilibrium geometry. Thus, we define the scaling factor as

$$\alpha = \frac{d_{CC} + r^B_{eq}}{a_{Cl} + a_\Phi} \tag{4.29}$$

and the new cavity radii and solvation energies (denoted by primes after rescaling) are

$$a' = \alpha a \tag{4.30}$$

$$\Delta G'_{s,eq}(r') = \alpha \Delta G_{s,eq}(r') = -\frac{\alpha q^2}{2\alpha a}\left(1 - \frac{1}{\epsilon}\right) = \Delta G_{s,eq}(r) \tag{4.31}$$

Therefore, the equilibrium solvation energies are

$$\Delta G'^B_{s,eq} = -\frac{\alpha}{2}\left(1 - \frac{1}{\epsilon}\right)\left(\frac{(q^B_{Cl})^2}{a'_{Cl}} + \frac{(q^B_\Phi)^2}{a'_\Phi} + \frac{2q^B_{Cl}q^B_\Phi}{d_{CC} + r^B_{eq}}\right)$$

$$\Delta G'^A_{s,eq}(r') = -\frac{\alpha}{2}\left(1 - \frac{1}{\epsilon}\right)\left(\frac{[q^A_{Cl}(r'/\alpha)]^2}{a'_{Cl}} + \frac{[q^A_\Phi(r'/\alpha)]^2}{a'_\Phi} + \frac{2q^A_{Cl}q^A_\Phi}{d_{CC} + r'}\right) \tag{4.32}$$

Note that eq 4.32 defines the $^2A_1$ and $^2B_1$ state equilibrium solvation free energies for the anion system at the equilibrium geometry of the $^2B_1$ state, i.e., at $r = r^B_{eq}$. As we have already discussed, we are ignoring any possible dependence of the equilibrium polarization for the $^2B_1$ state on the C−Cl bond extension, largely because of the smallness of q^B_{Cl}. The situation is more complicated for the $^2A_1$ state. As discussed in Section 4.2.1, there is a charge redistribution between the ring C atom and the Cl atom in the $^2A_1$ state as r increases. We have taken this important effect into account, and it provides the major r dependence for $\Delta G^A_{s,eq}$ on the bond extension that is carried along in the formulation equations eq 4.17 and 4.32. Otherwise, much less important sources of r dependence that are associated with the changing physical location of a charged Cl moiety and the induced solvent displacement are discussed in ref 101.

Finally, we note that, with the $^2A_1$ and $^2B_1$ charges defined as previously noted, the charge transfer between the $^2B_1$ and $^2A_1$ states is fractional: $\Delta q(r) = q^B_{Cl} - q^A_{Cl}(r)$, $\Delta q(r^B_{eq}) \simeq 0.4$. This transfer factor will occur explicitly in the nonequilibrium solvent reorganization free energy, which is discussed next.

4.2.3. Nonequilibrium Solvation Reorganization Energies. The nonequilibrium solvation components, $\lambda_s(s - s_{eq}(r))^2$, of the diabatic free energies shown in eq 4.17, involve the reorganization free energy λ_s, which, with eqs 4.15, 4.16, and 4.25, is given by

$$\lambda_s = \frac{1}{2}\left(\frac{1}{\epsilon_\infty} - \frac{1}{\epsilon}\right)\int d\boldsymbol{x}\,[\boldsymbol{E}^A(\boldsymbol{x}; r_{eq}^B) - \boldsymbol{E}^B(\boldsymbol{x}; r_{eq}^B)]^2 \qquad (4.33)$$

and, by eq 4.19, because $s_{eq}^B(r) = 0$, only the equilibrium position $s_{eq}^A(r)$ must be evaluated and this involves the r-dependent analogue of eq 4.33:

$$\lambda_s(r) = \frac{1}{2}\left(\frac{1}{\epsilon_\infty} - \frac{1}{\epsilon}\right)\int d\boldsymbol{x}\,[\boldsymbol{E}^A(\boldsymbol{x}; r) - \boldsymbol{E}^B(\boldsymbol{x}; r)]^2 \qquad (4.34)$$

Again, the presence of the difference of the inverses of the high-frequency and static dielectric constants reflects the feature that the reorganization is associated exclusively with the orientational polarization.

When the integrals within the Marcus−Hush cavity model framework are evaluated,[102] the two reorganization energies are

$$\lambda_s(r) = \left(\frac{1}{\epsilon_\infty} - \frac{1}{\epsilon}\right)\left\{\frac{[q_{Cl}^B - q_{Cl}^A(r)]^2}{2a_{Cl}} + \frac{[q_\Phi^B - q_\Phi^A(r)]^2}{2a_\Phi} + \frac{[q_{Cl}^B - q_{Cl}^A(r)][q_\Phi^B - q_\Phi^A(r)]}{d_{CC} + r}\right\}$$

$$\lambda_s = \lambda_s(r = r_{eq}^B) \qquad (4.35)$$

where d_{CC} is the distance between the center of the ring and the C atom (which has been determined by ab initio calculations to be $d_{CC} = 1.41$ Å) and a_{Cl} and a_Φ are the cavity radii determined previously (they are assumed not to vary with the charge present in the cavity). After the rescaling procedure, as described in Section 4.2.1, these become

$$\lambda'_s(r) = \alpha\left(\frac{1}{\epsilon_\infty} - \frac{1}{\epsilon}\right)\left(\frac{[q_{Cl}^B - q_{Cl}^A(r)]^2}{2a'_{Cl}} + \frac{[q_\Phi^B - q_\Phi^A(r)]^2}{2a'_\Phi} + \frac{[q_{Cl}^B - q_{Cl}^A][q_\Phi^B - q_\Phi^A(r)]}{d_{CC} + r}\right)$$

$$\lambda'_s = \lambda'_s(r = r_{eq}^B) \qquad (4.36)$$

As we noted at the end of Section 4.2.2, no r-dependent screening effects are included in the reorganization energy expressions. The origin of the r dependence here, beyond that which occurs from the r-dependent charge distribution in the $^2A_1$ state, is the fact that the cost of the charge transfer from the $^2B_1$ state to the $^2A_1$ state is dependent on the transfer distance, which increases as r increases.[103]

5. Reaction Rate Constants in Solution

We now address the calculation of the reaction rate constant for the $[CN-\Phi-Cl]^{\bullet-}$ dissociation in solution. We use the approach and the parameters that have been presented previously in the three solvents (water, acetonitrile, and DMF). After discussion of the rate-constant formulation, we initially explore the variation of those parameters and the solvent to examine how sensitive the resulting transition state (TS) locations and barrier heights are. Using the most likely parameter choices, we then compare the predicted rate constants with experimental results.

5.1. Rate-Constant Formulation. The first step is the calculation of the adiabatic ground-state free-energy surface $G(r,\theta,s)$, using eqs 4.3 and 4.15−4.19, with the vacuum potentials $V^{B,A}$ (given in eq 4.4), the electronic coupling β (from eq 4.2), the equilibrium solvation free energies $\Delta G_{s,eq}^{B,A}$ (evaluated according to eq 4.32), and the reorganization energies λ_s and $\lambda_s(r)$ (the latter of which enters the equilibrium solvent position $s_{eq}^A(r)$ via eq 4.20), evaluated according to eq 4.36.

TABLE 7: Influence of the Cavity Sizes (a_Φ and a_{Cl}), the Magnitude of the Charge Transfer ($\Delta q(r \to \infty)$), and the Charge on the Cyano Engroup (q_{CN}) on $\Delta G^\ddagger$ in Water, Acetonitrile (MeCN), and Dimethyl Formamide (DMF)[a]

case	solvent	ϵ_0	a_Φ (Å)	a_{Cl} (Å)	Δq (e)	q_{CN} (e)	$\Delta G^\ddagger$ (kcal/mol)
a	water	78.4	2.65	1.97	0.88	−0.28	9.7
b	water	78.4	2.87	2.18	0.88	−0.28	10.1
c	water	78.4	2.65	1.97	0.85	−0.28	8.8
d	water	78.4	2.65	1.97	0.88	−0.20	11.8
e	MeCN	37.5	2.85	2.21	0.88	−0.28	10.2
f	DMF	36.7	2.90	2.25	0.88	−0.28	9.9
g	DMF	36.7	3.00	2.25	0.88	−0.28	9.6

[a] $k_\theta = 23$ cal/deg^2 and $b = 0.62$ kcal/deg. The term $\Delta q(r \to \infty)$ represents the charge transfer from the reactant to the final product. See text for the description of the various cases. Some selected transition-state (TS) locations are reported in Table 8.

Next, the TS on this surface is located (see II), and, in each solvent, the molecule is bent at the TS, because of conical intersection point (CIP) avoidance; the reactant (R) minimum also is located. Finally, the rate constant is calculated via transition state theory (TST). The basic program is similar to that used previously for events such as S_N1 dissociations,[45b,c] proton transfer,[45a] and excited-electronic-state intramolecular charge-transfer reactions.[46]

According to TST as applied to our three-coordinate system and discussed in detail in II, the reaction rate constant is

$$k = 2\frac{\omega_{||}^R}{2\pi}\frac{\omega_{\perp 1}^R}{\omega_{\perp 1}^\ddagger}\frac{\omega_{\perp 2}^R}{\omega_{\perp 2}^\ddagger}\exp\left(-\frac{\Delta G^\ddagger}{RT}\right) \qquad (5.1)$$

where $\omega_{||}^R$ is the frequency along the reaction coordinate in the R region, whereas $\omega_{\perp 1}^R$ and $\omega_{\perp 2}^R$ are the frequencies for the two modes transverse to the reaction coordinate in the R region and at the TS. We have defined $\Delta G^\ddagger$ to be the difference of the free-energy values at the TS and the R minimum.[104] We recall from Section 4.1 that it is a free energy, rather than an energy, because of the many degrees of freedom of the solvent molecule that are implicit in the solvent coordinate.

The full details of the pre-exponential frequency factors in the rate-constant expression in eq 5.1 will be discussed in II. Here, we simply combine them into one prefactor, A_{sol}:

$$k = A_{sol}\exp\left(-\frac{\Delta G^\ddagger}{RT}\right) \qquad (5.2)$$

As we will see, the A_{sol} factor is approximately the same for the solvents considered ($A_{sol} = 1.6 \times 10^{13}$ s^{-1}) and is reasonably similar to its vacuum analogue (cf Table 4). Thus, we focus on the most sensitive factor for k: the $\Delta G^\ddagger$ factor.

5.1.1. Exploration of Model Parameter Sensitivity of $\Delta G^\ddagger$. 5.1.1.1. The Wag Force Constant k_θ and the Coupling Parameter b. We have already studied the influence of k_θ and b on the vacuum reaction barrier height in Section 3.3. For our solution calculations, we will keep the most likely values: the force constant in the $^2A_2$ state, which is $k_\theta = 23$ cal/deg^2, and the linear increase of the coupling, which is $b = 0.62$ kcal/deg.

5.1.1.2. The Cavity Sizes. Case a in Table 7 gives the results for the water solvent, using the hydration free energy values employed for Table 5. However, other estimates exist for the hydration free energies,[105] which leads to larger Cl and ring cavity radii. The result is presented in case b in Table 7, which

TABLE 8: Transition-State Coordinates, Prefactor A_{Sol}, Free Energy Barrier $\Delta G^{\ddagger}$, and Calculated and Experimental Rate Constants k and k^{Exp} for [CN−Φ−Cl]•⁻ Dissociation in Water, Acetonitrile (MeCN), and Dimethyl Formamide (DMF) Solvents

	value		
parameter	case a (water)	case e (MeCN)	case f (DMF)
ϵ_0	78.4	37.5	36.7
ϵ_∞	1.78	1.80	2.04
$r^{\ddagger}$ (Å)	2.04	2.05	2.05
$\theta^{\ddagger}$ (deg)	26	26	26
$s^{\ddagger}$	0.50	0.52	0.51
A_{sol} ($\times 10^{13}$ s^{-1})	1.6	1.6	1.6
$\Delta G^{\ddagger}$ (kcal/mol)	9.7	10.2	9.9
k_{300K} ($\times 10^6$ s^{-1})	1.5	0.5	0.9
k^{exp}_{300K} ($\times 10^6$ s^{-1})	5−17[a]	50−500[b]	160−450 (±90)[c]

[a] From refs 13 and 72. [b] From refs 73 and 71. [c] From refs 8 and 12.

leads to a barrier height increase of ∼0.4 kcal. This direction is understandable, in terms of the decreased solvation for increased radii, which is more important for the charge-localized Cl atom.

The ring cavity sizes in DMF and acetonitrile in Table 5 have been approximately determined from the solvation free energies of anions that have similar hydration free energies. The consequence of this uncertainty on the barrier properties for the DMF reaction is detailed in Table 7: the larger ring cavity in case g, compared to that in case f, leads to a smaller solvation of the (predominantly $^2B_1$ state) R, compared to the TS, which is a mixture of $^2B_1$ and $^2A_1$ states, and, thus, a slightly reduced $\Delta G^{\ddagger}$ result.

5.1.1.3. Influence of the Diabatic Charge Distributions. Section 4.2.1 showed that the determination of the partial charges in both $^2A_1$ and $^2B_1$ states—and, therefore, the charge-transfer magnitude—is not unambiguous. We recall here that this magnitude is $\Delta q(r \rightarrow \infty)$, i.e., from the reactant to the final product.

In case c in Table 7, the magnitude of the charge transfer is decreased, with respect to case a, from $\Delta q = 0.88$ to $\Delta q = 0.85$. The consequence on the barrier height is a decrease of ∼0.9 kcal.[106]

We now examine the influence of the charge located on the cyano endgroup. In our model, this charge is approximated to be fixed, and equal, for the $^2B_1$ and $^2A_1$ states (cf. Section 4.2.2). In case d in Table 7, the cyano endgroup charge q_{CN} is decreased from −0.28 to −0.20, whereas the charge-transfer magnitude Δq and the Cl charges are kept constant; this amounts to changing the fraction of the ring charge that is withdrawn by the cyano group. Decreasing the fraction of the charge fixed on the cyano group implies that the charge shared by the "active" parts of the system (the ring and the Cl) is increased. The barrier height consequence is an increase of ∼2.1 kcal/mol. Indeed, the larger ring charge stabilizes the $^2B_1$ state, with respect to the $^2A_1$ state, because the $^2B_1$ solvation free energy is mainly due to the solvation of the ring.

5.1.1.4. Influence of Solvent Polarity. A comparison of Tables 4 and 8 shows that the solution activation barriers are, in all cases, lower than the vacuum energy barrier, and that the TS location of the C−Cl bond extension ($r^{\ddagger}$) is smaller in solution than that in the vacuum. These are associated trends, which are ultimately related to the better solvation of the anion system in its dissociative $^2A_1$ state, with the charge localized on the Cl^- anion, compared to the bound $^2B_1$ state with the charged delocalized in the ring system; in increasingly polar solvents, the CI location moves toward smaller r values, and thus toward lower energies, because of this differential solvation. Related behavior should be expected, more generally, for CIs that involve states with differing charge distributions.

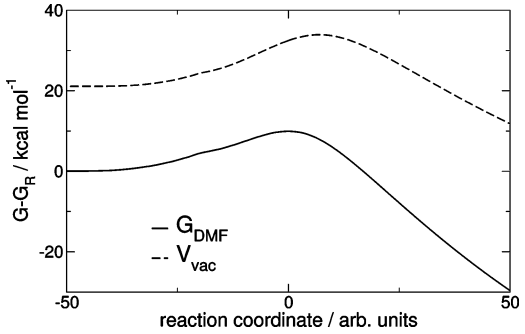

Figure 6. Free energy in DMF and vacuum potential energy profiles along the [CN−Φ−Cl]•⁻ dissociation reaction path.

Figure 6 shows the free energy for the calculated reaction path in DMF, together with the potential energy along the (virtual) vacuum reaction path. Although the R, TS, and product are all greatly stabilized by the solvent, the net solution barrier is only slightly reduced (by 2.9 kcal/mol), compared to the gas phase. The TS occurs earlier, consistent with the Hammond postulate, which is further pursued below.

Actually, although useful, the aforementioned diabatic perspective explanation is quite crude, given the fact that the electronic coupling that produces the adiabatic free-energy surface is very large at the bent TS, which is characterized by a finite wag angle, $\theta^{\ddagger}$. A more proper explanation would be in terms of the electronic structure of the adiabatic TS, the stabilization of the contact ion pair (CIP) product and the Hammond postulate, as follows.

The electronic composition of the TS for the three solvent reactions can be determined from eq 4.4, with the results being $[c^B(r^{\ddagger},\theta^{\ddagger},s^{\ddagger})]^2 = 0.63$, 0.61, and 0.62 in water, acetonitrile, and DMF, respectively, compared to the vacuum value (0.52). The important solvation of the $^2B_1$ state component of the electronic structure of the TS species reduces the barrier compared to that in the vacuum. The CIP product is even more stabilized, compared to that in the vacuum, because the charge on Cl is more fully developed: $(c^B_{CIP})^2 = 0$, and the reaction free energies for the three solvents, defined from the reactants to the CIP, are −73, −70, and −73 kcal/mol, respectively. Consistent with the Hammond postulate, the TS will be progressively earlier. Interestingly, this TS electronic structure variation, as in other examples[45b,45c,46] is not consistent with other proposals[107] that it should remain fixed at a value of $^1/_2$.

5.1.2. Comparison with Experiment. The experimental rate constants for [CN−Φ−Cl]•⁻ measured in water, acetonitrile, and DMF are reported in Table 8.

Our best estimate (using the raw parameters extracted from the calculations in Table 2 and the experimental solvation energies detailed in Section 4.2.1) is case a, for which $k = 1.5 \times 10^6$ s^{-1} in water. This rate constant is similar to the range defined by the two available rates, $k = 5 \times 10^6$ s^{-1} and $k = 17 \times 10^6$ s^{-1}. In acetonitrile and DMF, our best estimates are, respectively, case e, for which $k = 0.5 \times 10^6$ s^{-1}, and case f, for which $k = 0.9 \times 10^6$ s^{-1}, which are both reasonably similar to the available experimental determinations. However, cases b, c, d, and g show that the uncertainty on these values is large (at least an order of magnitude).

From the theoretical rate constants just listed, the reaction seems to be slightly accelerated by a more polar solvent. This trend, although not pronounced, is consistent with the picture of the $^2A_1$ state being preferentially stabilized with respect to

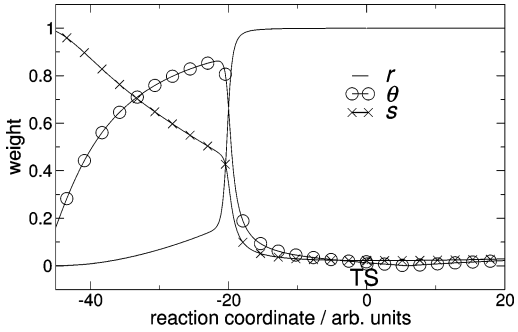

Figure 7. Dissociation of [CN−Φ−Cl]•⁻ in DMF (case f), showing the contribution of each (mass-weighted) coordinate to the reaction coordinate *r*, *θ*, and *s* along the reaction path.

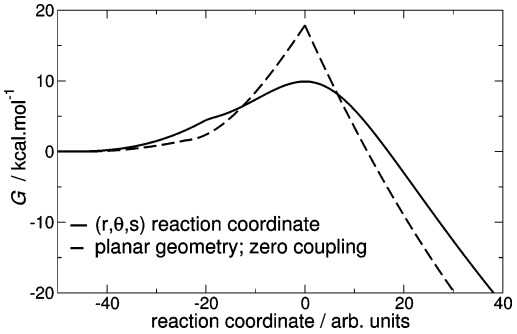

Figure 8. Free-energy profiles along the (*r*,*θ*,*s*) reaction coordinates, and along the path restricted to planar geometry, with no electronic coupling, for [CN−Φ−Cl]•⁻ in DMF (case f). The reaction free energy is $\Delta_r G \simeq -70$ kcal/mol.

the $^2B_1$ state in a more polar solvent, implying a decrease of the free-energy barrier (see Section 5.1.1). The polarity trend of the experimental rates in Table 8 seems to be in the opposite direction. However, the change in the rate-constant values between DMF, acetonitrile, and water (e.g., approximately an order of magnitude) is too small, compared to the experimental uncertainty (an order of magnitude for the measurements in acetonitrile), to be significant. (Furthermore, related recent experiments do not observe a polarity dependence.[108]) In addition, those rates have been measured by different groups with different methods, and this renders the comparison more difficult. We would recommend a re-examination of those experimental results. On the other hand, in our treatment, the description of the solvent by a dielectric continuum with solute cavities whose sizes must be determined semiempirically for each solvent is obviously a heavy approximation. The influence of solvent polarity on the rates should be re-examined with molecular dynamics simulations.[109]

5.2. Comparison with Previous Work. We will discuss many more details of the reaction rate constant, as well as the reaction path, in II. Here, we limit ourselves to an exposition of those aspects that are connected solely to a comparison with the only previous theoretical formulation for radical anion dissociation in solution, which is due to Savéant.[2] The latter formulation shares some general features with the present work. For example, bound-state and dissociative-state model potentials in the separation coordinate *r* were used (although not informed by ab initio calculations), and solvent reorganization was included (although in a fashion appropriate for outer-sphere electron transfers). Two quite significant differences are that (i) the C−Cl wag angle was not explicitly included and its impact on the barrier height was neglected,[110] although its role in allowing the dissociation was clearly recognized, and (ii) the explicit numerical impact of the electronic coupling on the barrier height (and reaction path) was neglected. The explicit incorporation of the wag angle and the electronic coupling provides essential ingredients in our formulation; therefore, here, we present some results that have been obtained using the methods of II, which are addressed specifically to the consequences of these aspects.

We begin in Figure 7, which has information about the three-dimensional reaction path for the anion dissociation in DMF (calculated in II). This figure represents the contribution of each of the coordinates (*r*,*θ*,*s*) to the reaction path leading from the R to the TS with bent geometry. The pathway portrayed—and explained in II, in terms of the various time scales for these coordinates—is a path that, initially, is dominated by the reorganization of the solvent (i.e., motion in *s*), followed by an adjustment of the bending angle *θ*, and finally followed in the immediate neighborhood of the TS by the C−Cl stretch motion in *r*. The required reorganization of *θ* and *s* to reach the required TS values—for the first, to avoid the CIP, and for the second, to provide the requisitive solvation for the TS charge distribution—is largely completed before the major part of this final stretching. (As we will see in II, the reaction paths vary in important aspects for the other solvents water and acetonitrile.)

Figure 8 compares the free-energy profiles of [CN−Φ−Cl]•⁻ in DMF calculated along the reaction coordinate, explained in II in terms of the three dimensions *r*, *θ*, and *s* (Figure 8a), and along the path restricted to planar geometry $\theta = 0$, and thus with no electronic coupling (Figure 8b). The barrier in the latter case is significantly higher (≃8 kcal/mol) than that in the former, which is a pattern that has also been observed for the other two solvents considered. Focusing solely on the most significant aspects of this difference, we note that, in our formulation (illustrated in Figure 8), the wag angle is significant ($\theta^{\ddagger} = 26°$) at the TS and the electronic coupling at this value is quite large ($\beta(\theta^{\ddagger}) = 16$ kcal/mol).[111] Beyond the feature that, in Figure 8, the TS is not located at the same *r* (or *s*) values in the two descriptions, the large difference between the barrier heights (8 kcal/mol) is a result of the stabilizing effect on the ground-state adiabatic surface by the electronic coupling (see ref 112 on the additional effect of solvent-induced coupling), together with the smaller destabilizing effect that is due to the energy cost to bend the C−Cl bond, i.e., just those ingredients responsible for the fact that the solution reaction path (II), when viewed in the *r* and *θ* coordinates, corresponds to motion in the moat avoiding the CIP, just as in the gas phase (Figure 4). We continue to examine these issues below.

5.2.1. Free Energy Profile along s and r at the Transition State. We noted in the Introduction that the current strong electronic coupling anion dissociation is to be distinguished from the situation for more weak-coupling outer-sphere electron transfer (ET) reactions. The differences are many, but Figures 9 and 10 show especially important ones.

In Figure 9, the free energy is shown as a function of the solvent coordinate in the neighborhood of the TS value of *s* ($s^{\ddagger}$), all with *r* and *θ* values at their TS values $r^{\ddagger}$ and $\theta^{\ddagger}$, respectively. The TS solvent coordinate $s^{\ddagger}$ is a local minimum. On the other hand, if, at these TS $r^{\ddagger},\theta^{\ddagger}$ values, the electronic coupling were ignored, as in standard ET perspectives, the pair of solvent parabolas result (and there is no longer any solvent minimum). In the latter view, an activated ET process in the solvent coordinate would be involved. Clearly, the current adiabatic and a standard ET description are significantly different.

In Figure 10, the free energy is shown as a function of the C−Cl distance *r* in the TS neighborhood, with *θ* and *s* being fixed at their TS values $\theta^{\ddagger}$ and $s^{\ddagger}$, respectively. In the adiabatic

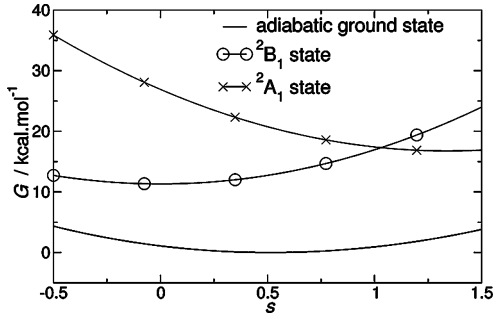

Figure 9. Free-energy profile along the solvent coordinate, with the solute in its transition-state (TS) geometry ($r^{\ddagger},\theta^{\ddagger}$), in the adiabatic ground state and in each diabatic state, for [CN−Φ−Cl]•⁻ in DMF (case f). The free-energy origin is $G(r^{\ddagger},\theta^{\ddagger},s^{\ddagger})$.

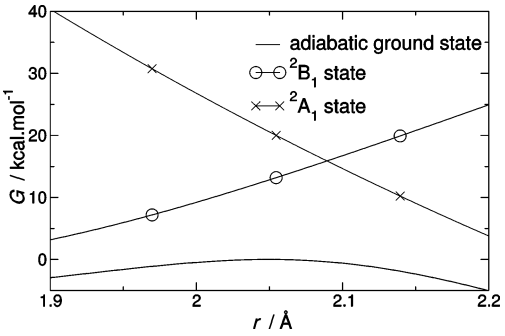

Figure 10. Free-energy profile along r in the TS neighborhood, with $(\theta,s) = (\theta^{\ddagger},s^{\ddagger})$, in the adiabatic ground state and in each diabatic state, for [CN−Φ−Cl]•⁻ in DMF (case f). The free-energy origin is $G(r^{\ddagger},\theta^{\ddagger},s^{\ddagger})$.

ground state, the system goes over a barrier along r. On the other hand, if the electronic coupling vanishes, the picture is that of two crossing curves, again strongly contrasting the present adiabatic perspective with that of ET.

5.2.2. Anion Bond Dissociation Energy. The considerations just discussed indicate the very strong difference between the predictions where the electronic coupling (and the associated C−Cl wagging motion) are neglected, and when they are included. However, it is a very striking result that, in the former type of treatment, Savéant[2] has been able to determine that the activation free energy for the thermodynamically symmetric reaction ($\Delta_r G = 0$), the so-called intrinsic barrier $\Delta G_0^{\ddagger}$, should vary with the homolytic bond dissociation energy D of the radical anion ($[Ar{-}X]\bullet^- \rightarrow [Ar\bullet]\bullet^- + \bullet X$) and a solvent reorganization energy that, here, is called λ. In particular, the intrinsic barrier height was predicted to be[2]

$$\Delta G_0^{\ddagger} = \frac{D+\lambda}{4} \tag{5.3}$$

The intrinsic barriers were extracted from rate data for non-symmetric reactions via the quadratic relation of the Marcus type, as derived by Savéant:[2]

$$\Delta G^{\ddagger} = \Delta G_0^{\ddagger}\left(1 + \frac{\Delta_r G}{4\Delta G_0^{\ddagger}}\right)^2 \tag{5.4}$$

The predicted linear dependence on D of the intrinsic barriers so extracted was observed to be in very good general agreement with experiment.[2,24]

An important question is then: does our treatment, which explicitly includes the strong electronic coupling and the wag coordinate neglected in the Savéant treatment, show this type of dependence on D? Our [CN−Φ−Cl]•⁻ reaction results in three solvents do not provide a wide range; therefore, we have chosen to address this question in the following manner.

Our strategy is to vary D artificially about its [CN−Φ−Cl]•⁻ value, separately in the vacuum and in DMF, in such a way that the reaction free energy remains constant. To do this conveniently, we must somewhat alter the vacuum potential forms given in eq 2.6, such that the $^2A_1$ repulsive curve is described as in the Savéant model:[2]

$$\begin{aligned} V^{\mathrm{B}}(r,\theta=0) &= V_0^{\mathrm{B}} + D\{1 - \exp[-a(r - r_{\mathrm{eq}}^{\mathrm{B}})]\}^2 \\ V^{\mathrm{A}}(r,\theta=0) &= V_0^{\mathrm{A}} + D\exp[-2a(r - r_{\mathrm{eq}}^{\mathrm{B}})] \\ &= V_0^{\mathrm{A}} + D\exp(2ar_{\mathrm{eq}}^{\mathrm{B}})\exp(-2ar) \end{aligned} \tag{5.5}$$

The connection with the parameters of eq 2.6 is the following:

$$\begin{aligned} D_{\mathrm{e}}^{\mathrm{B}} &= D \\ D_{\mathrm{e}}^{\mathrm{A}} &= D\exp(2ar_{\mathrm{eq}}^{\mathrm{B}}) \\ a^{\mathrm{B}} &= a \\ a^{\mathrm{A}} &= 2a \end{aligned} \tag{5.6}$$

In this formulation, the $^2B_1$ and $^2A_1$ state bond dissociation energies are proportional, and scaling the parameter D implies scaling the dissociation energies of both states by the same amount.

With the modification shown in eq 5.5, we then calculate the rate constants in the vacuum and in DMF, for various values of D, using exactly our entire theoretical development used to predict the rates in Tables 4 and 8. All these reactions are asymmetric: in the vacuum, the reaction free energy is $\Delta_r V = V_0^{\mathrm{A}} - V_0^{\mathrm{B}} \simeq -45.5$ kcal/mol, and in DMF, the equilibrium solvation increases the asymmetry to $\Delta_r G = (V_0^{\mathrm{A}} + \Delta G_{\mathrm{s,eq}}^{\mathrm{A}}) - (V_0^{\mathrm{B}} + \Delta G_{\mathrm{s,eq}}^{\mathrm{B}}) \simeq -73$ kcal/mol.

For our comparison in the vacuum, for each value of D, $\Delta V_0^{\ddagger}$ is obtained in two different ways. First, we use our model with the explicit wag coordinate θ and a nonvanishing coupling. The TS is located on the two-dimensional (r,θ) reaction surface, and $\Delta V_0^{\ddagger}$ is calculated as the R−TS potential-energy difference for the symmetric reaction. The other route is via the Savéant−Marcus relations given in eqs 5.3 and 5.4, where, in the latter, there is obviously no solvent reorganization contribution for the vaccum reaction, and only potential energy is involved. This yields, in fact, the potential-energy difference between the tip of the CI and the reactant. The two sets of $\Delta V_0^{\ddagger}$ results displayed in Figure 11 are approximately linear in D; however, the comparison shows that, in the (r,θ) picture, the wag allows access to a TS that is lower in energy, because of the avoidance of the CI tip, which is due to the wagging motion.

In DMF, we compare two different ways of obtaining $\Delta G_0^{\ddagger}$. First, it is (properly) calculated as the free-energy difference between the TS and the R on our three-dimensional (r,θ,s) surface. A second determination is provided by the Savéant−Marcus relationships presented in eqs 5.3 and 5.4. Figure 12 shows the important point that the present treatment yields an approximately linear relation between $\Delta G_0^{\ddagger}$ and D. The other determination yields values of $\Delta G_0^{\ddagger}$, which are approximately linear with D, but the value obtained is considerably larger than that in the full picture.

5.2.3. Activation Free Energies. We have already drawn attention in our discussion of Figures 9 and 10 to the fact that

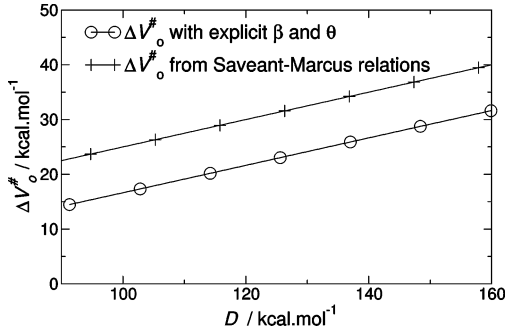

Figure 11. Comparison of $\Delta V_0^{\ddagger}$ obtained from our picture with explicit coupling β and angular coordinate θ, and from the Marcus−Savéant relationships presented in eqs 5.3 and 5.4 for different bond dissociation energies (D) in the vacuum.

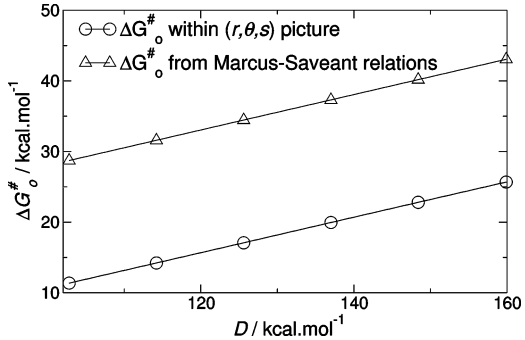

Figure 12. Comparison of the intrinsic activation free energy $\Delta G_0^{\ddagger}$ obtained from our picture with explicit coupling β and angular coordinate θ and the $\Delta G_0^{\ddagger}$ value obtained from the Marcus−Savéant relationships presented in eqs 5.3 and 5.4 for different bond dissociation energies (D) in DMF. Note: for [CN−Φ−Cl]•⁻, D = 114 kcal/mol, but the corresponding $\Delta G_0^{\ddagger}$ value reported here is not the one that we have determined in DMF, because our analytical model is based on the fits of the ab initio potentials, and these fits cannot be reproduced by the restrictive form of Savéant's model potentials that are given in eq 5.5: our potentials do not fulfill the condition described in eq 5.6.

the barrier heights estimated in the absence of the electronic coupling and wag motion are in considerable excess (≃8 kcal) than those calculated in our theory; this excess is approximately composed of the magnitude of the electronic coupling minus the wagging potential energy, both evaluated at the TS. This same sort of excess is also evident in Figures 11 and 12 at any D value considered. Here, we analyze the situation more explicitly.

To proceed, we re-express the adiabatic system free energy G, presented in eq 4.3, in the form (we suppress the (r,θ,s)-dependent notation)

$$G = (c^{\mathrm{B}})^2 G^{\mathrm{B}} + (c^{\mathrm{A}})^2 G^{\mathrm{A}} - 2c^{\mathrm{B}}c^{\mathrm{A}}\beta \tag{5.7}$$

in terms of the population factors, the diabatic free energies $G^{\mathrm{B,A}}$, and the coupling β. Here, we have used the $^2B_1$- and $^2A_1$-state populations $(c^{\mathrm{B}})^2$ and $(c^{\mathrm{A}})^2$, given in eq 4.4, in the adiabatic wave function, and the relation

$$c^{\mathrm{B}}c^{\mathrm{A}} = \sqrt{(c^{\mathrm{B}})^2(c^{\mathrm{A}})^2} = \frac{\beta}{\sqrt{(G^{\mathrm{A}} - G^{\mathrm{B}})^2 + 4\beta^2}} \tag{5.8}$$

With eq 4.17, we then have

$$G = (c^{\mathrm{B}})^2 G_{\mathrm{eq}}^{\mathrm{B}} + (c^{\mathrm{A}})^2 G_{\mathrm{eq}}^{\mathrm{A}} + \lambda_s[(c^{\mathrm{B}})^2 s^2 + (c^{\mathrm{A}})^2 (s - s_{\mathrm{eq}}^{\mathrm{A}})^2] - 2c^{\mathrm{B}}c^{\mathrm{A}}\beta \tag{5.9}$$

where the equilibrium diabatic free energies $G_{\mathrm{eq}}^{\mathrm{B,A}}$ consist of the vacuum potentials and the equilibrium solvation free energies: $G_{\mathrm{eq}}^{\mathrm{B,A}} = V^{\mathrm{B,A}} + \Delta G_{\mathrm{s,eq}}^{\mathrm{B,A}}$.

A discussion of the thermodynamically symmetric reaction will suffice to make the basic point. The TS will be located, by symmetry, at $G^{\mathrm{B}} = G^{\mathrm{A}}$, with $(c^{\mathrm{B}})^2 = (c^{\mathrm{A}})^2 = {}^1/_2$, and eq 5.9 reduces at the TS to

$$G^{\ddagger} = G_{\mathrm{eq}}^{\mathrm{B}\,\ddagger} + \frac{1}{4}\Lambda - \beta^{\ddagger} \tag{5.10}$$

where we have defined a solvent reorganization term Λ:

$$\Lambda = 2\lambda_s[s^{\ddagger 2} + (s^{\ddagger} - s_{\mathrm{eq}}^{\mathrm{A}\,\ddagger})^2] \tag{5.11}$$

If, for simplicity, we ignore the r dependence of $s_{\mathrm{eq}}^{\mathrm{A}\,\ddagger}$ (see eq 4.19) and s_{eq} (see eq 4.20), then this reduces to the simple result $2\lambda_s\{({}^1/_2)^2 + [({}^1/_2) - 1]^2\} = \lambda_s$.

In the R, we can safely assume, as a good approximation, that the composition is pure B, i.e., $(c^{\mathrm{B}})^2 = 1$, $(c^{\mathrm{A}})^2 = 0$, and $s = 0$ (see eq 4.19), so that, from eq 5.9, we have $G_{\mathrm{R}} = G_{\mathrm{eq}}^{\mathrm{B}}$ at the B reactant geometry. The intrinsic barrier height for the symmetric reaction then is

$$\Delta G_0^{\ddagger} = G^{\ddagger} - G_{\mathrm{R}} = [V^{\mathrm{B}}(r^{\ddagger},\theta^{\ddagger}) - V^{\mathrm{B}}(r_{\mathrm{eq}}^{\mathrm{B}},\theta = 0)] + \frac{1}{4}\Lambda - \beta^{\ddagger} \tag{5.12}$$

where we have used the fact that, in our model, the equilibrium solvation free energy of B does not change between the R and TS locations: $\Delta G_{\mathrm{s,eq}}^{\mathrm{B}\,\ddagger} - \Delta G_{\mathrm{s,eq}}^{\mathrm{B}}(r_{\mathrm{eq}}^{\mathrm{B}}) = 0$.

The result shown in eq 5.12 shows two important things. First, within the approximations stated, the contribution of the C−Cl bond stretching contained in the expression $[V^{\mathrm{B}}(r^{\ddagger},\theta^{\ddagger}) - V^{\mathrm{B}}(r_{\mathrm{eq}}^{\mathrm{B}},\theta = 0)]$ is proportional to D, where D is the anion homolytic bond dissociation energy. This explains the linear correlation with D observed in our theory of the intrinsic barrier (see Figure 12). Second, the *excess* over this $\Delta G_0^{\ddagger}$ value of the intrinsic barrier $\Delta G_0^{\ddagger\prime}$ ($\Delta\Delta G_0^{\ddagger} = \Delta G_0^{\ddagger\prime} - \Delta G_0^{\ddagger}$), which one would infer by ignoring the wag and the electronic coupling, is then

$$\Delta\Delta G_0^{\ddagger} \simeq \beta^{\ddagger} - [V^{\mathrm{B}}(\theta^{\ddagger}) - V^{\mathrm{B}}(\theta = 0)] \tag{5.13}$$

which explicitly shows the difference that has been previously discussed qualitatively: the electronic coupling minus the cost of the wag to reach the TS value of θ.

This explains why the experimental intrinsic barriers[12] $\Delta G_0^{\ddagger}$ are much smaller than the $(D + \lambda)/4$ value that is predicted by eq 5.3. The intrinsic barrier should not be interpreted, as suggested in ref 12, as being mainly constituted by the solvent reorganization energy, with a negligible geometric reorganization energy corresponding to a significant electronic density already in the $^2B_1$ state. Numerically, for [CN−Φ−Cl]•⁻ in DMF, $V^{\mathrm{B}}(\theta^{\ddagger}) - V^{\mathrm{B}}(\theta = 0)$ = 21.2 kcal/mol, Λ = 10.7 kcal/mol, $\beta^{\ddagger}$ = 16.2kcal/mol, which shows that the geometric reorganization energy is far from being negligible. In addition, our resulting intrinsic barrier value $\Delta G_0^{\ddagger}$ = 7.7 kcal/mol is in good agreement with the experimental result[12] of 5.7 kcal/mol.

6. Concluding Remarks

In this paper, we have developed a theoretical description for the dissociation of aromatic radical anions in solution, illustrated for [CN−Φ−Cl]•⁻ in water, acetonitrile, and di-

methyl formamide (DMF) solvents. A key and novel component is the treatment of the conical intersection (CI) aspects of the reaction. In particular, the C−Cl wag motion is critical in avoiding the CI and, thus, generating strong electronic coupling—between the diabatic bound and dissociative states—which allows the charge flow from the ring system onto the departing Cl atom and results in a bent transition state (TS). The required electronic structure information was provided by ab initio calculations. The strong coupling of the reaction to the surrounding polar solvent was included via the explicit introduction of a solvent coordinate, with attention to the central nonequilibrium solvation feature: the solvent does not have time to equilibrate to the C−Cl stretch and bending motions as the reaction proceeds.

The entire formulation was couched in analytic terms, culminating in expressions for the dissociation reaction rate constant. Evaluation in the three solvents gave results that were in fair agreement with experiment, given the uncertainties in the latter. This success suggests that the present formulation could be useful for other ground-state CI-dominated dissociations (see, for example, ref 43). The relatively modest increase of the rate constant with increasing solvent polarity ($\simeq$1 order of magnitude) suggests that major changes in rate constants from one molecule/solvent system to another are likely to be dominated by molecular changes, which implies different electronic coupling and state ordering effects (see Sections 2.2 and 2.3).

Analysis of the rate constants—and, in particular, analysis of the activation free energies—showed that the inclusion of the wagging motion and the resulting strong electronic coupling has a very important impact on the reaction barrier; without this effect, the barrier almost doubles, from $\simeq$9.7 kcal to $\simeq$18 kcal. This contrasts with the neglect of this feature in the pioneering theoretical model that was reported by Savéant. However, the Savéant model first pinpointed the important correlation of the barrier height with the homolytic bond dissociation energy of the anion; this experimentally confirmed correlation is also shown by the present theory.

The present treatment is approximate, and several improvements within this present formulation could be made. Examples include inclusion of the C−Cl bond-length-distance dependence of the electronic coupling and attention to a varying screening of the Cl solvation as the dissociation proceeds. These will not change the basic picture but probably will have some relatively minor numerical consequences.[113] A more significant extension of interest would be to include a microscopic treatment of the solvent, rather than the somewhat crude dielectric continuum model that has been applied within. In this connection, one must remember that the electronic structure issues must be simultaneously addressed. One possibility would be to maintain the diabatic description of the present work, augmented by calculations to determine the r dependence of the electronic coupling, and to combine that with the type of molecular dynamics computer simulation used successfully for, e.g., S_N1 dissociation.[45f,114a,114b] For this purpose, one would have to define a microscopic analogue of the type of solvent coordinate we have used within both to find the TS region and to examine the dynamics in its neighborhood. In other bond-breaking and bond-making reaction problems, one can define such a coordinate,[114] which is related to the difference of the full microscopic Hamiltonians, including the solvent molecule's contributions, for the reaction system in the two diabatic states, and it seems likely that one could do the same for the anion dissociation problem, using the $^2A_1$ and $^2B_1$ diabatic states.

Beyond its role in $S_{R,N}1$ nucleophilic substitution, radical anion dissociation is also implicated in the formation mechanism of Grignard reagents, which is of considerable significance in organic synthesis. Two mechanisms are envisaged, which differ in the decay channel for the radical anion $[R-X]\bullet^-$ intermediate: it can either dissociate or be reduced by the magnesium metallic surface to form a dianion.[5] Accordingly, an analysis of the present type for the lifetime of aromatic radical anions in solution could help decide between those mechanisms.

Furthermore, our analysis should also be relevant for halogenated uracil (halo-uracil) compounds[6] that are involved in DNA damage. Halo-uracils are widely used in radiation therapy, where they are incorporated in DNA in place of thymine bases to enhance the DNA sensivity to radiation and increase the death of proliferating cells. The ionizing radiation produces secondary electrons and their attachment to halo-uracil leads to the dissociation $[U-X]\bullet^- \rightarrow U\bullet + X^-$, producing the uracil radical $U\bullet$, which causes breaks in the DNA strand. The detailed mechanism is not yet well understood; however, recent calculations that are associated with the present research indicate the occurrence of a CI in the chloro-uracil dissociation.[115]

Finally, aspects of the present formulation could prove useful for the study of photochemical dynamics for radical anions in solution;[11] however, the nature of the states that are excited requires clarification,[11] and further theoretical developments for the dynamical passage through CIs in solution will be required.

Acknowledgment. This work was supported in part by the CNRS, the Forschergruppe Niederenergetische Elektronenstreuung (DFG), and the National Science Foundation (under NSF Grant CHE-0108314. We thank Stefan Grimme (University of Münster), both for useful discussions and for preliminary calculations on the chlorobenzene radical anion; Phil Kiefer (University of Colorado, Boulder), for initial discussions on this problem; Christian Amatore (ENS), for introducing us to the problem; and Michel Chanon (University of Aix−Marseille), for informing us of the relevance for Grignard reactions.

References and Notes

(1) (a) Kornblum, N. *Angew. Chem., Int. Ed. Engl.* **1975**, *14*, 734−735. (b) Russel, G. A. *Adv. Phys. Org. Chem.* **1987**, *23*, 271. (c) Bunnett, J. F. *Acc. Chem. Res.* **1978**, *11*, 413−420. (d) Bowman, W. R. *Chem. Soc. Rev.* **1988**, *17*, 283−316. (e) Rossi, R. A.; de Rossi, R. H. *Aromatic Substitution by the $S_{RN}1$ Mechanism*; ACS Monograph 178; American Chemical Society: Washington, DC, 1983. (f) Rossi, R. A.; Pierini, A. B.; Penenory, A. B. *Chem. Rev.* **2003**, *103*, 71−167. (g) Eberson, L. *Electron-Transfer Reactions in Organic Chemistry*; Springer−Verlag: New York, 1987.

(2) Savéant, J.-M. *J. Phys. Chem.* **1994**, *98*, 3716−3724.

(3) Savéant, J.-M. *Adv. Phys. Org. Chem.* **1990**, *26*, 1−130.

(4) Savéant, J.-M. *Tetrahedron* **1994**, *50*, 10117−10165.

(5) (a) Garst, J. F.; Boone, J. R.; Webb, L.; Lawrence, K. E.; Baxter, J. T.; Ungváry, F. *Inorg. Chim. Act.* **1999**, *296*, 52−66. (b) Garst, J. F.; Ungváry, F. *Grignard Reagents: New Developments*; Richey, H. G., Ed.; Wiley−Interscience: New York, 2000. (c) Bodineau, N.; Mattalia, J.-M.; Thimokhin, V.; Handoo, K.; Négrel, J.-C.; Chanon, M. *Org. Lett.* **2000**, *2*, 2303−2306. (d) Berg, U.; Bodineau, N.; Négrel, J.-C.; Mattalia, J.-M.; Timokhin, V.; Handoo, K.; Marchi, C.; Chanon, M. *C. R. Acad. Sci., Ser. IIc: Chim.* **2001**, *4*, 567−570.

(6) (a) Abdoul-Carime, H.; Huels, M.; Illenberger, E.; Sanche, L. *J. Am. Chem. Soc.* **2001**, *123*, 5354−5355. (b) Li, X.; Sanche, L.; Sevilla, M. D. *J. Phys. Chem. A* **2002**, *106*, 11248−11253. (c) Abdoul-Carime, H.; Huels, M. A.; Brüning, F.; Illenberger, E.; Sanche, L. *J. Chem. Phys.* **2000**, *113*, 2517−2521. (d) Boudaiffa, B.; Cloutier, P.; Hunting, D.; Huels, M. A.; Sanche, L. *Science* **2000**, *287*, 1658−1660. (e) Fujimoto, K.; Ikeda, Y.; Saito, I. *Tetrahedron Lett.* **2000**, *41*, 6455−6459. (f) Denifl, S.; Matejcik, S.; Gstir, B.; Hanel, G.; Probst, M.; Scheier, P.; Märk, T. D. *J. Chem. Phys.* **2003**, *118*, 4107−4114.

(7) Amatore, C.; Combellas, C.; Pinson, J.; Oturan, M. A.; Robveille, S.; Savéant, J.-M.; Thiébault, A. *J. Am. Chem. Soc.* **1985**, *107*, 4846−4853.

(8) Andrieux, C. P.; Savéant, J.-M.; Zann, D. *Nouv. J. Chim.* **1984**, *8*, 107−116.
(9) Amatore, C.; Oturan, M. A.; Pinson, J.; Savéant, J.-M.; Thiébault, A. *J. Am. Chem. Soc.* **1985**, *107*, 3451−3459.
(10) Chesta, C. A.; Cosa, S. S.; Previtali, C. M. *J. Photochem. Photobiol. A: Chem.* **1989**, *45*, 9−15.
(11) (a) Compton, R. G.; Dryfe, R. A. W.; Fisher, A. C. *J. Electroanal. Chem.* **1993**, *361*, 275−278. (b) Compton, R. G.; Dryfe, R. A. W.; Fisher, A. C. *J. Chem. Soc., Perkin Trans. 2* **1994**, *7*, 1581−1587. (c) Compton, R. G.; Dryfe, R. A. W. *J. Electroanal. Chem.* **1994**, *375*, 247−255. (d) Compton, R. G.; Dryfe, R. A. W.; Eklund, J. C.; Page, S. D.; Hirst, J.; Nei, L.; Fleet, G. W. J.; Hsia, K. Y.; Bethell, D.; Martingale, L. J. *J. Chem. Soc., Perkin Trans. 2* **1995**, *8*, 1673−1677.
(12) Enemaerke, R. J.; Christensen, T. B.; Jensen, H.; Daasbjerg, K. *J. Chem. Soc., Perkin Trans. 2* **2001**, *9*, 1620−1630.
(13) Neta, P.; Behar, D. *J. Am. Chem. Soc.* **1981**, *103*, 103−106.
(14) Neta, P.; Behar, D. *J. Am. Chem. Soc.* **1980**, *102*, 4798−4802.
(15) Behar, D.; Neta, P. *J. Am. Chem. Soc.* **1981**, *103*, 2280−2283.
(16) (a) Kimura, N.; Takamuku, S. *Bull. Chem. Soc. Jpn.* **1986**, *59*, 3653−3654. (b) Kimura, N.; Takamuku, S. *J. Am. Chem. Soc.* **1995**, *117*, 8023−8024.
(17) Takeda, N.; Poliakov, P. V.; Cook, A. R.; Miller, J. R. *preprint*.
(18) (a) Wentworth, W. E.; Becker, R. S.; Tung, R. *J. Phys. Chem.* **1967**, *71*, 1652−1665. (b) Steelhammer, J. C.; Wentworth, W. E. *J. Chem. Phys.* **1969**, *51*, 1802−1814.
(19) Jordan, K. D.; Michejda, J. A.; Burrow, P. D. *J. Am. Chem. Soc.* **1976**, *98*, 7189−7191.
(20) Olthoff, J. K.; Tossell, J. A.; Moore, J. H. *J. Chem. Phys.* **1985**, *83*, 5627−5634.
(21) Stricklett, K. L.; Chu, S. C.; Burrow, P. D. *Chem. Phys. Lett.* **1986**, *131*, 279−284.
(22) (a) Symons, M. C. R. *J. Chem. Soc., Faraday Trans. 1* **1981**, *77*, 783−790. (b) Symons, M. C. R.; Bowman, W. R. *J. Chem. Soc., Perkin Trans.* **1987**, *8*, 1133−1138.
(23) Savéant, J.-M. *Acc. Chem. Res.* **1993**, *26*, 455−461.
(24) Costentin, C.; Robert, M.; Savéant, J.-M. *J. Am. Chem. Soc.* **2003**, *125*, 105−112.
(25) (a) Pierini, A. B.; Duca, J. S., Jr. *J. Chem. Soc., Perkin Trans. 2* **1995**, *9*, 1821−1828. (b) Pierini, A. B.; Duca, J. S., Jr.; Vera, D. M. A. *J. Chem. Soc., Perkin Trans. 2* **1999**, *5*, 1003−1009.
(26) (a) Villar, H.; Castro, E. A.; Rossi, R. A. *Can. J. Chem.* **1982**, *60*, 2525−2527. (b) Moreno, M.; Gallardo, I.; Bertrán, J. *J. Chem. Soc., Perkin Trans. 2* **1989**, *2*, 2017−2021.
(27) Benassi, R.; Bertarini, C.; Taddei, F. *Chem. Phys. Lett.* **1996**, *257*, 633−638.
(28) Clarke, D. D.; Coulson, C. A. *J. Chem. Soc. A* **1969**, *1*, 169−172.
(29) Chanon, M.; Rajzmann, M.; Chanon, F. *Tetrahedron* **1990**, *46*, 6193−6299.
(30) Konovalov, V. V.; Laev, S. S.; Beregovaya, I. V.; Shchegoleva, L. N.; Shteingarts, V. D.; Tsvetkov, Y. D.; Bilkis, I. *J. Phys. Chem. A* **2000**, *104*, 352−361.
(31) Beregovaya, I. V.; Shchegoleva, L. N. *Chem. Phys. Lett.* **2001**, *348*, 501−506.
(32) Skalický, T.; Collet, C.; Pasquier, N.; Allan, M. *Phys. Chem. Chem. Phys.* **2002**, *4*, 3583−3590.
(33) Blancafort, L.; Jolibois, F.; Olivucci, M.; Robb, M. A. *J. Am. Chem. Soc.* **2001**, *123*, 722−732.
(34) (a) Vreven, T.; Bernardi, F.; Garavelli, M.; Olivucci, M.; Robb, M. A.; Schlegel, H. B. *J. Am. Chem. Soc.* **1997**, 12687−12688. (b) Garavelli, M.; Bernardi, F.; Olivucci, M.; Vreven, T.; Klein, S.; Celani, P.; Robb, M. A. *Faraday Discuss.* **1998**, *110*, 51−70. (c) Bernardi, F.; Olivucci, M.; Robb, M. A. *J. Photochem. Photobiol. A: Chem.* **1997**, *105*, 365−371. (d) Robb, M. A.; Olivucci, M. *J. Photochem. Photobiol. A: Chem.* **2001**, *144*, 237−243.
(35) Molnar, F.; Ben-Nun, M.; Martínez, T. J.; Schulten, K. *THEOCHEM* **2000**, *506*, 169−178.
(36) Bersuker, I. B.; Polinger, V. Z. *Vibronic Interactions in Molecules and Crystals*; Springer: Berlin, 1989.
(37) Cattaneo, P.; Granucci, G.; Persico, M. *J. Phys. Chem. A* **1999**, *103*, 3364−3371.
(38) Salem, L. *Electrons in Chemical Reactions: First Principles*; Wiley−Interscience: New York, 1982.
(39) (a) Yarkony, D. R. *J. Phys. Chem.* **1996**, *100*, 18612−18628. (b) Yarkony, D. R. *Rev. Mod. Phys.* **1996**, *68*, 985−1013.
(40) (a) Michl, J.; Klessinger, M. *Excited States and Photochemistry of Organic Molecules*; VCH: New York, 1995. (b) Michl, J.; Bonačič-Koutecký, V. *Electronic Aspects of Organic Photochemistry*; Wiley: New York, 1990.
(41) (a) Sobolewski, A. L.; Domcke, W. *Chem. Phys.* **2000**, *259*, 181−191. (b) Domcke, W.; Stock, G. *Adv. Chem. Phys.* **1997**, *100*, 1−169. (c) Woywod, C.; Domcke, W.; Sobolewski, A. L.; Werner, H.-J. *J. Chem. Phys.* **1994**, *100*, 1400−1413. (d) Köppel, H.; Domcke, W.; Cederbaum, L. S. *Adv. Chem. Phys.* **1984**, *57*, 59−246. (e) Thiel, A.; Köppel, H. *J. Chem. Phys.* **1999**, *110*, 9371−9383. (f) Raab, A.; Worth, G.; Meyer, H.-D.; Cederbaum, L. S. *J. Chem. Phys.* **1999**, *110*, 936−946.
(42) (a) Blancafort, L.; Adam, W.; González, D.; Olivucci, M.; Vreven, T.; Robb, M. A. *J. Am. Chem. Soc.* **1999**, *121*, 10583−10590. (b) Sinicropi, A.; Pogni, R.; Basosi, R.; Robb, M. A.; Gramlich, G.; Nau, W. M.; Olivucci, M. *Angew. Chem., Int. Ed.* **2001**, *113*, 4313−4318.
(43) Lorance, E. D.; Kramer, W. H.; Gould, I. R. *J. Am. Chem. Soc.* **2003**, *124*, 15225−15238.
(44) Laage, D.; Burghardt, I.; Sommerfeld, T.; Hynes, J. T. *ChemPhysChem* **2003**, *4*, 61−66.
(45) (a) Juanos-i-Timoneda, J.; Hynes, J. T. *J. Phys. Chem.* **1991**, *95*, 10431−10442. (b) Kim, H. J.; Hynes, J. T. *J. Am. Chem. Soc.* **1992**, *114*, 10508−10528. (c) Kim, H. J.; Hynes, J. T. *J. Am. Chem. Soc.* **1992**, *114*, 10528−10537. (d) Bianco, R.; Hynes, J. T. *J. Chem. Phys.* **1995**, *102*, 7885−7901. (e) Gertner, B. J.; Ando, K.; Bianco, R.; Hynes, J. T. *Chem. Phys.* **1994**, *183*, 309−323. (f) Benjamin, I.; Barbara, P.; Gertner, B. J.; Hynes, J. T. *J. Phys. Chem.* **1995**, *99*, 7557−7567. (g) Mathis, J. R.; Bianco, R.; Hynes, J. T. *J. Mol. Liq.* **1994**, *61*, 81−102. (h) Peslherbe, G. H.; Bianco, R.; Hynes, J. T.; Ladanyi, B. M. *Faraday Trans. 2* **1997**, *93*, 977−988.
(46) (a) Fonseca, T.; Kim, H. J.; Hynes, J. T. *J. Mol. Liq.* **1994**, *60*, 161−200. (b) Kim, H. J.; Hynes, J. T. *J. Photochem. Photobiol. A: Chem.* **1997**, *105*, 337−343.
(47) Kim, H. J.; Hynes, J. T. *J. Chem. Phys.* **1992**, *96*, 5088−5110.
(48) (a) Marcus, R. A. *Angew. Chem., Int. Ed. Engl.* **1993**, *32*, 1111−1121. (b) Newton, M. D.; Sutin, N. *Annu. Rev. Phys. Chem.* **1984**, *35*, 437−480. (c) Cannon, R. D. *Electron-Transfer Reactions*; Butterworth: London, 1980.
(49) The radical anion dissociation reaction contrasts with other outer-sphere, non-adiabatic electron-transfer reactions, where the influence of conformational transition on the electron transfer has already been studied. (See, for example, Matyushov, D. V. *Chem. Phys. Lett.* **1993**, *203*, 131−136.)
(50) Borosky, G. L.; Nishimoto, S.-I.; Pierini, A. B. *THEOCHEM* **2000**, *499*, 151−160.
(51) Wetmore, S. D.; Boyd, R. J.; Eriksson, L. A. *Chem. Phys. Lett.* **2001**, *343*, 151−158.
(52) Modelli, A.; Venuti, M. *J. Phys. Chem. A* **2001**, *105*, 5836−5841.
(53) Burghardt, I.; Laage, D.; Hynes, J. T. *J. Phys. Chem. A* **2003**, *107*, 11292−11306.
(54) Nicolaides, A.; Smith, D. M.; Jensen, F.; Radom, L. *J. Am. Chem. Soc.* **1997**, *119*, 8083−8088.
(55) Jordan, K. D.; Burrow, P. D. *Acc. Chem. Res.* **1978**, *11*, 341−348.
(56) Stockdale, J. A.; Hurst, G. S.; Christophorou, L. G. *Nature* **1964**, *202*, 459−461.
(57) Note that, in electron transmission spectroscopy (ETS) experiments on the gas-phase species,[19] it has been shown that the dissociation process ("dissociative electron attachment") may weakly interfere, despite its long time scale as compared with that for electron detachment.
(58) A recent experimental study showed that, in tetrahydrofuran (THF), the fluorobenzene radical anion exists in equilibrium with the solvated electron; however, the radical anion is more stable than the solvated electron form. (See Marasas, R. A.; Iyoda, T.; Miller, J. R. *J. Phys. Chem. A* **2003**, *107*, 2033−2038).
(59) Coulson et al.[28] also raised the issue of the initial geometry of the radical anion, after formation by electron attachment. In our approach, we neglect vibrational relaxation, which should be fast, compared to the reactive process, provided the latter has a noticeable barrier.
(60) Burrow, P. D.; Modelli, A.; Chiu, N. S.; Jordan, K. D. *Chem. Phys. Lett.* **1981**, *82*, 270−276.
(61) Indeed, in group theory terms, a given vibration couples two electronic states when the direct product of the irreducible representations Γ_1 and Γ_2 of the two states, with that of the vibration Γ_{vib} contains the totally symmetric representation Γ_A, i.e., $\Gamma_1 \times \Gamma_{vib} \times \Gamma_2 \supset \Gamma_A$. The out-of-plane wag has B_1 symmetry; therefore, it couples the $^2B_1$ and $^2A_1$ diabatic states, because $\Gamma_{B_1} \times \Gamma_{B_1} \times \Gamma_{A_1} = \Gamma_{A_1}$.
(62) Other vibrational modes, e.g., in-plane vibrations or out-of-plane deformations, couple the $^2A_2$ state with the $^2B_1$ and $^2A_1$ states; however, these couplings are much weaker than those between the $^2B_1$ and $^2A_1$ states.[32]
(63) Laage, D. *Theoretical Studies of Charge-Transfer Reactions in Solution*; Thesis, University Paris VI, Paris, France, 2001.
(64) Many additional aspects of the chlorobenzene radical anion are discussed in ref 63.
(65) Potts, A. W.; Edvardsson, D.; Karlsson, L.; Holland, D. M. P.; MacDonald, M. A.; Hayes, M. A.; Maripuu, R.; Siegbahn, K.; von Niessen, W. *Chem. Phys.* **2000**, *254*, 385−405.
(66) This clearly contradicts the results of AM1 semiempirical calculations, both from previous work (ref 25a) and work repeated in this study (ref 63), which instead predict a stable bent anion. Semiempirical methods do not seem to be reliable for these anionic systems.
(67) The lack of a planar equilibrium geometry, or even the absence of a minimum, are not incompatible with our model. We use *diabatic* states with planar equilibrium geometry, and this does not necessarily imply that the *adiabatic* states have their equilibrium geometry at $\theta = 0$. In the presence

of a vibronic coupling, the equilibrium geometry of a molecule may be distorted, as is typically the case for Jahn−Teller-type systems (see ref 41d).

(68) The addition of a substituent has other effects on the reaction barrier, besides the evoked inductive and resonance effects. See, for example, the discussion in ref 43, even though it misses precisely the inductive and resonance aspects.

(69) For polysubstituted aromatic radical anions, the rationale for the preference of one leaving group over another is based on the homolytic bond dissociation energy of the anionic compound (see refs 12 and 63) and not on that of the neutral.

(70) Tanner, D. D.; Chen, J. J.; Chen, L.; Luelo, C. *J. Am. Chem. Soc.* **1991**, *113*, 8074−8081.

(71) Andrieux, C. P.; Blocman, C.; Dumas-Bouchiat, J. M.; M'Halla, F.; Savéant, J. M. *J. Am. Chem. Soc.* **1980**, *102*, 3806−3813.

(72) Geppert, W. D.; Getoff, N.; Sehested, K.; Holcman, J. *Radiat. Phys. Chem.* **2000**, *59*, 39−47.

(73) Penn, J. H.; Cox, E. D. *J. Org. Chem.* **1986**, *51*, 4447−4449.

(74) The CN substituent alsolies in the aromatic plane, in contrast with the acetonitrile radical anion situation. (See Shkrob, I. A.; Takeda, K.; Williams, F. *J. Phys. Chem. A* **2002**, *106*, 9132−9144.)

(75) Meot-Ner, M.; Neta, P.; Norris, R. K.; Wilson, K. *J. Phys. Chem.* **1986**, *90*, 168−173.

(76) More properly, we should refer here to a "pseudo" gas-phase model, because we use a modified vacuum Hamiltonian where autoionization is inhibited.

(77) These CI problems are sometimes classified, in a general sense, as Jahn−Teller (JT)-type systems, in contrast with Renner−Teller, or as glancing intersections, characterized by quadratic couplings (see ref 39). The JT Hamiltonian, as such, is a highly symmetric example of a vibronic-coupling system that involves a linear coupling (see ref 41d). In particular, the so-called $E \times \epsilon$ JT Hamiltonian describes the coupling of a two-fold degenerate electronic state to a degenerate vibration, in nonlinear molecules.[41d]

(78) A crude estimate was performed for the neutral chlorobenzene, using the semiempirics, varying θ with $r_{\Phi-Cl}$ fixed. No quartic component appeared, and the potential seemed harmonic, even for wag angles as large as 90°.

(79) See, for example, Uzer, T.; Hynes, J. T.; Reinhardt, W. P. *J. Chem. Phys.* **1986**, *85*, 5791−5804 and Uzer, T.; Hynes, J. T.; Reinhardt, W. P. *Chem. Phys. Lett.* **1985**, *177*, 600−605.

(80) Fontanesi, C. *THEOCHEM* **1997**, *392*, 87−94.

(81) (a) Riss, U. V.; Meyer, H.-D. *J. Phys. B—At. Mol. Opt.* **1993**, *26*, 4503−4536. (b) Sommerfeld, T.; Riss, U. V.; Meyer, H.-D.; Cederbaum, L. S.; Engels, B.; Suter, H. *J. Phys. B—At. Mol. Opt.* **1998**, *31*, 4107−4122.

(82) Molcas Version 5, University of Lund, Sweden, 2000.

(83) Dunning, T. H., Jr. *J. Chem. Phys.* **1970**, *53*, 2823.

(84) Koopmans, T. *Physica* **1933**, *1*, 104−113.

(85) Santra, R.; Cederbaum, L. S.; Meyer, H.-D. *Chem. Phys. Lett.* **1999**, *303*, 413−419.

(86) The value of k_θ in the chlorobenzene radical anion (given in ref 63) is very similar, and the presence of the cyano substituent in [CN−Φ−Cl]•⁻ has little effect on the local −Cl bending-mode frequency. However, a small increase of the wag force constant with the addition of an electron withdrawing substituent is expected, as discussed in ref 43.

(87) Test calculations showed that including the *r*-dependence of μ_θ did not change the reaction path, and μ_θ was fixed to its TS value for simplicity.

(88) Rettig, W. *Angew. Chem., Int. Ed. Engl.* **1986**, *25*, 971−988.

(89) The more general situation where nonadiabatic effects are important is discussed in ref 63.

(90) See, for example, (a) Hynes, J. T. The Theory of Reactions in Solution. In *Theory of Chemical Reaction Dynamics*; Baer, M., Ed.; CRC Press: Boca Raton, FL, 1985; Vol. IV, Chapter 4. (b) Steinfeld, J. I.; Francisco, J. S.; Hase, W. L. *Chemical Kinetics and Dynamics*, 2nd ed. Prentice Hall: Upper Saddle River, NJ, 1999.

(91) (a) Cramer, C. J.; Truhlar, D. G. *J. Comput.-Aided Mol. Design* **1992**, *6*, 629−666. (b) Cramer, C. J.; Truhlar, D. G. *Chem. Rev.* **1999**, *99*, 2161−2200. (c) Klamt, A.; Schüürmann, G. *J. Chem. Soc., Perkin Trans. 2* **1993**, *5*, 799−805. (d) Tomasi, J.; Persico, M. *Chem. Rev.* **1994**, *94*, 2027−2094.

(92) Borgis, D.; Hynes, J. T. *Chem. Phys.* **1993**, *170*, 315−346.

(93) The solvent also introduces an off-diagonal contribution in the representation (eq 4.2), because there is a finite transition moment between the two diabatic states, and this leads to a solvent-induced electronic coupling contribution.[47] (This issue will be addressed in Section 5.2.)

(94) The description given in eq 4.2 corresponds to a particular limiting description of the electronic (rather than nuclear) polarization of the solvent. The characteristic frequency for the solvent electronic polarization response to any electron transfer can be characterized by $\hbar\omega_{el}$, where $\hbar\omega_{el}$ is approximately the solvent's electronic absorption frequency of the solvent (see ref 47). When the two $^2B_1$ and $^2A_1$ diabatic states are in resonance, i.e., where $G^B = G^A$, the frequency of electron shuttle back and forth is governed by the electronic coupling $\beta(\theta)$. The description given in 4.2 applies when the solvent electronic polarization response is sufficiently fast enough compared to the electron shuttling time between the two diabatic states, such that the electronic polarization "sees" the individual diabatic state charge distributions (as opposed to "seeing" the resonant mixture of those charge distributions): $\beta(\theta)/(\hbar\omega_{el}) \ll 1$. This condition is approximately satisfied for the current systems: water, acetonitrile (MeCN), and dimethyl formamide (DMF) are all colorless, so $\hbar\omega_{el} > 70$ kcal.

(95) Bianco, R.; Hynes, J. T. *J. Chem. Phys.* **1995**, *102*, 7864−7884.

(96) (a) Thompson, W. H.; Hynes, J. T. *J. Am. Chem. Soc.* **2000**, *122*, 6278−6286. (b) Peslherbe, G. H.; Ladanyi, B. M.; Hynes, J. T. *J. Phys. Chem. A* **1998**, *102*, 4100−4110. (c) Mathis, J. R.; Kim, H. J.; Hynes, J. T. *J. Am. Chem. Soc.* **1993**, *115*, 8248−8262.

(97) More conventionally, one might refer to what we here term valence bond (VB) wave functions and states as "localized electron wavefunctions", which are to be coupled (mixed) to find molecular eigenstates. We thank J. Michl (University of Colorado) for a discussion on this point.

(98) (a) Lee, S.; Hynes, J. T. *J. Chem. Phys.* **1988**, *88*, 6853−6862. (b) Lee, S.; Hynes, J. T. *J. Chem. Phys.* **1988**, *88*, 6863−6869.

(99) Dewar, M. J. S.; Zoebisch, E. G.; Healy, E. F.; Stewart, J. J. P. *J. Am. Chem. Soc.* **1985**, *107*, 3902−3909.

(100) AMPAC 5.0, Semichem: Shawnee, KS, 1994.

(101) The physical origin of another source of *r* dependence can be understood in terms of the "screening" provided by the physical presence of the ring system for the interaction of the Cl atom with the solvent. (For this discussion, we consider, for simplicity, the Cl species to have a fixed charge). Regardless of this degree of screening at the C−Cl bond length $r = r_{eq}^B$, it should decrease as the C−Cl bond is stretched, and when *r* is large enough, it should vanish, leaving the Cl atom interacting with the solvent unimpaired by the presence of the ring. The latter limit is never reached in our considerations, because the entire development is restricted to *r* up to and somewhat beyond the transition state (TS). This effect should not be of great importance in the *r* range of interest for the rate constant. In any event, any such screening effect is neglected in the form of the reorganization energy that we will develop in the next subsection, and it also is ignored here, for consistency. Another source of *r* dependence is related to the solvent displacement during the dissociation process. As shown in a similar situation in an S_N2 reaction in water (see Gertner, B. J.; Whitnell, R. M.; Wilson, K. R.; Hynes, J. T. *J. Am. Chem. Soc.* **1991**, *113*, 74−87), the solvent displacement by the Cl moiety can be ignored in comparison with the solvent polarization effects associated with an increasing C−Cl bond length, and in any case, is only a potential problem at large *r* values past the TS, which is not the focus of this paper.

(102) (a) Marcus, R. A. *J. Chem. Phys.* **1956**, *24*, 966−978. (b) Hush, N. S. *Trans. Faraday Soc.* **1961**, *4*, 557.

(103) Mathematically, it arises from the cross term in eq 4.34 between the A and B electric fields, and there is no such term in the equilibrium solvation free-energy equation (eq 4.26).

(104) Other definitions of an activation free energy can be found in the literature. Many discusssions of a TST rate constant are expressed in the form $k = (k_BT/h)\exp[-\Delta G^{\ddagger}_{TST}/(k_BT)]$ (see ref 90), in which $\Delta G^{\ddagger}_{TST}$ contains various contributions of nonreactive degrees of freedom at the transition state (TS) and various degrees of freedom in the reactants (R). The obvious connection of such a $\Delta G^{\ddagger}_{TST}$ to our $\Delta G^{\ddagger}$ is, from eq 5.2, $\Delta G^{\ddagger}_{TST} = \Delta G^{\ddagger} + RT\ln[k_BT/(hA)]$.

(105) Pearson, R. G. *J. Am. Chem. Soc.* **1986**, *108*, 6109−6114.

(106) Interestingly, this decrease is larger than the expected decrease, which is proportional to $(\Delta q'/\Delta q)^2$. Indeed, a change in the charge transfer has an equilibrium and a nonequilibrium effect. First, a reduction of magnitude of the charge transfer implies a smaller solvent reorganization energy, and the nonequilibrium portion of the activation free energy decreases. However, there is also an equilibrium barrier reduction effect, as now described. In our description, the final product-state charge distribution is well-defined: there is a full negative charge on the Cl^- anion, and the remaining aromatic radical is neutral. Thus, a reduction of charge transfer implies less charge on the ring system, and because this charge dominates the equilibrium solvation free energy of the reactant, there is less reactant equilibrium solvation stabilization, and the free energy barrier rises.

(107) (a) Pross, A.; Shaik, S. S. *Acc. Chem. Res.* **1983**, *16*, 363−370. (b) Pross, A. *Acc. Chem. Res.* **1985**, *18*, 21−219. (c) Shaik, S. S. *Prog. Phys. Org. Chem.* **1985**, *15*, 197−337.

(108) Recent pulse radiolysis experiments on a related compound—para-chloro-biphenyl radical anion—did not show any noticeable polarity dependence of the rate constant (see ref 17).

(109) Laage, D., Hynes, J. T., work in progress.

(110) The wagging motion is less critical in the related benzylic aromatic anion class, for which a detailed validation of Savéant's model was performed (Andrieux, C. P.; Le Gorande, A.; Savéant, J.-M. *J. Am. Chem. Soc.* **1992**, *114*, 6892−6904). A CI exists in planar geometry (Fontanesi, C.; Baraldi, P.; Marcaccio, M. *THEOCHEM* **2001**, *548*, 13−20), similar to that for phenylic compounds; however, the equilibrium geometry is already bent, thus providing a nonvanishing coupling and allowing a faster dissociation (see ref 52).

(111) This value of the TS coupling is much larger than that in a previous estimate (see Adcock, W.; Andrieux, C. P.; Clark, C. I.; Neudeck, A.; Savéant, J.-M.; Tardy, C. *J. Am. Chem. Soc.* **1995**, *117*, 8285−8286) and cannot be neglected.

(112) The solvent renormalization contribution β_S to the electronic coupling will be governed by (i) the transition moment between the diabatic states involved, $^2B_1$ and $^2A_1$ in the present problem (the moment should be perpendicular to the aromatic plane, via symmetry arguments) and (ii) the equilibrium solvent polarization (see ref 47). First, we consider the effect of this contribution at the solution transition state (TS). If this β_S contribution were to have the same angle dependence as that of the vacuum contribution in eq 2.4, i.e., $\beta_S = b_S\theta$, then a simple analysis using the angle potential $^1/_2k_\theta\theta^2$ and the renormalized coupling $(1 + b_S/b)b\theta$ shows that the TS reduction from the CI point would be increased over the results presented in the beginning of Section 5.2 (approximately $-^1/_2b^2/k_\theta$ by the factor $(1 + b_S/b)^2$. If b_S/b were as much as 30%,[47] this would be a significant enhancement in the TS reduction of ≃70%. (This is, however, likely an overestimate, because the angle at the TS is increased by the factor $(1 + b_S/b)$, and positive θ potential anharmonicity likely becomes important, reducing the predicting TS angle.) In the other limit, if β_S were angle-independent, then, the estimate given in the text in Section 5.2 for the reduction would not be altered, because β_S would reduce the CI and the TS by equal amounts. But if β_S were indeed finite at $\theta = 0$, there would no longer be a conical intersection for $\theta = 0$ in solution: the $^2B_1$ and $^2A_1$ curves would be split by $2\beta_S$. Such a splitting, although not essential for the present ground-electronic-state problem, would be of potential significance for the excited electronic state to ground-state transition, i.e., in the usual context of the interest in CIs as photochemical funnels (see refs 33−41). Unfortunately, we are presently unable to estimate either the magnitude or the θ dependence of the required transition moment reliably. The difficulty is that no computational methodology currently exists to calculate such moments with CAPS (cf. Section 3.1), and one would be forced to use a small confining basis set, which is generally unreliable. We are currently exploring calculation methods to address this issue, which are also necessary to investigate the solvent renormalization of the coupling effect on the reaction activation free energies.

(113) The chlorobenzene radical anion—which we rejected as a paradigm molecule in Section 2.3—presents a puzzle, on the very existence of the stable anion in solution. Namely, experimental rate constants for its dissociation in solution have been reported;[10] however, it is not clear at this moment how a stable chlorobenzene radical anion with a lifetime of more than approximately a picosecond can exist in solution. For further discussion, see ref 63.

(114) (a) Keirstead, W. P.; Wilson, K. R.; Hynes, J. T. *J. Chem. Phys.* **1991**, *95*, 5256−5267. (b) Gertner, B. J.; Hynes, J. T. *Faraday Discuss.* **1998**, *110*, 301−322. (c) Ando, K.; Hynes, J. T. *J. Mol. Liq.* **1995**, *64*, 25−37. (d) Ando, K.; Hynes, J. T. *J. Phys. Chem. B* **1997**, *101*, 10464−10478. (e) Ando, K.; Hynes, J. T. *J. Phys. Chem. A* **1999**, *103*, 10398−10408. (f) Ando, K.; Hynes, J. T. Acid−Base Proton Transfer and Ion Pair Formation in Solution. In *Advances in Chemistry and Physics*; Prigogine, I., Rice, S. A., Eds.; Wiley: New York, 1999; Vol. 110, Chapter 6, pp 381−430. (g) Staib, A.; Borgis, D.; Hynes, J. T. *J. Chem. Phys.* **1995**, *102*, 2487−2505.

(115) Sommerfeld, T. *ChemPhysChem* **2001**, *2*, 677−679.

(116) Because the energy gap is one of the important quantities in our model, we note that it may be approximately determined by calculations for the neutral molecule, by invoking Koopmans' theorem. This says that the orbital energies for the neutral give an estimate of the electron affinity and, hence, the energy of the anion. The estimate is reasonably good: at the equilibrium geometry of the neutral, $r = 1.74$ Å, the energies obtained using Koopmans' theorem are 2.1 eV (B_1), 2.9 eV (A_2), and 4.8 eV (A_1), to be compared with 1.7 eV (B_1), 2.1 eV (A_2), and 4.6 eV (A_1) from a calculation for the anion.

(117) Marcus, Y. *Ion Solvation*; Wiley−Interscience: New York, 1985.